



ELSEVIER

Contents lists available at ScienceDirect

Mechanical Systems and Signal Processing

journal homepage: www.elsevier.com/locate/ymssp

Physics-guided diagnosis framework for bridge health monitoring using raw vehicle accelerations

Yifu Lan, Zhenkun Li, Weiwei Lin^{*}

Department of Civil Engineering, Aalto University, 02150 Espoo, Finland

ARTICLE INFO

Communicated by: Dr. Spilios Fassois

Keywords:

Indirect SHM
Automated inspection
Damage detection
Vehicle-bridge interaction
Physics-guided model

ABSTRACT

Damage detection of bridges using vibrations from a passing vehicle has received a lot of interest recently. Though non-modal parameter-based methods (e.g., data-driven approaches) have shown promising results in this context, their advancement towards a comprehensive and rigorous monitoring system is hampered by their overreliance on machine learning techniques. On this background, this paper proposes a novel automatic physics-guided diagnosis framework for bridge health monitoring utilizing only raw vehicle accelerations. First, numerical studies are conducted to investigate the relationship between vehicle time-domain signals and bridge damage, based on which a new damage index is proposed. At the same time, it also explores the identification of damage locations and proposes a location index. Second, a damage diagnosis framework, which consists of a data processing method and a physics-guided model, is designed to overcome deficiencies from a drive-by measurement and to automate the damage detection process. The proposed framework was validated using datasets acquired from laboratory experiments employing a scale vehicle model and a steel beam. The results affirmed the method's efficacy in damage indication, quantification, and localization. Moreover, the superiority of the proposed damage index and the rationale for the proposed physics-guided approach were also demonstrated through comparisons with machine learning-based methods.

1. Introduction

Bridges represent a crucial component of civil infrastructure, contributing to the promotion of societal economic growth and living standards. However, bridge structural failure has increasingly become a global concern these days. In the United States, 42 % of all bridges have been in service for at least half a century, with structural deficiencies (such as material deterioration) identified in 46,154, or 7.5 %, of the country's bridges [1]. In Europe, the majority of bridges were built between 1945 and 1965, and many have recently faced aging and degradation issues [2]. Clearly, the development of effective bridge health monitoring systems capable of detecting damage at an early stage is of paramount importance. Due to the strategic goal of smart cities, robotic construction and automated inspection have become a trend recently [3–5].

Generally, conventional structural health monitoring (SHM) methods necessitate the placement of multiple sensors directly on the bridge [6]. The significant costs associated with on-site sensor installation and maintenance have long rendered such technology an expensive option [7]. Although the use of wireless sensors can reduce costs to some extent, a challenge in direct methods is that the instrumentation is often permanently affixed to the bridge, becoming a tailored SHM system for a specific bridge [8]. Transferring the

^{*} Corresponding author.

E-mail address: weiwei.lin@aalto.fi (W. Lin).

<https://doi.org/10.1016/j.ymssp.2023.110899>

Received 24 February 2023; Received in revised form 27 October 2023; Accepted 29 October 2023

0888-3270/© 2023 The Author(s). Published by Elsevier Ltd. This is an open access article under the CC BY license (<http://creativecommons.org/licenses/by/4.0/>).

monitoring framework to other bridges proves to be a challenging task. These obstacles hinder the widespread adoption of direct SHM technologies in bridges. Therefore, it is essential to develop a method that does not require instrumentation directly on bridges, which would significantly benefit engineering practice.

An indirect SHM approach, also known as the “drive-by inspection method” or “vehicle scanning method”, can provide a low-cost solution to bridge health monitoring problems. First introduced by Yang et al. [9], this approach utilizes the vehicle-bridge interaction (VBI) model to derive the bridge’s fundamental frequency from the dynamics of a traversing vehicle. The vehicle serves both as the exciter and the receiver, eliminating the need for direct bridge instrumentation [10]. Instead, sensors are mounted on the vehicle. Numerous studies have confirmed the potential to extract bridge modal parameters like frequencies and mode shapes from vehicle responses [11–25]. Changes in these parameters can hint at structural degradation [26], based on which the methods are referred to as modal parameter-based methods [27]. Yet, many such techniques struggle to detect minute damage or quantify damage [28]. Although there are methods that employ metrics like damping, displacement, and moving force, they too face challenges and often lack experimental validation [29–32]. Furthermore, modal parameter-based methods can be subjective, leaning on expert judgement, posing the risk of human bias, which is not in line with the trend towards automatic SHM in smart cities [3,33,34].

Recent years have seen a surge in non-modal parameter-based methods, notably data-driven approaches, for indirect SHM. Several studies have proven their potential for damage quantification. For instance, Lan et al. [35] accurately identified different bridge damage levels using vehicle vibration data via an optimized AdaBoost-linear Support Vector Machine (SVM). In 2019, Malekjafarian et al. [36] first applied Artificial Neural Networks (ANNs) to indirect SHM, achieving the detection of damage degrees. Although promising results have been obtained, they usually require a large number of labelled samples from varied damage states to fit the model (i.e., supervised learning), which is often impractical. As an example of non-supervised learning model, Liu et al. [37] utilized stacked autoencoders as dimensionality reduction methods to explore the full bandwidth frequency response, and then performed regression analysis on the extracted features for damage quantification. Similarly, Sarwar and Cantero [38] employed deep autoencoders as dimensionality reduction methods, combined with statistical distribution-based strategies, to quantify the bridge damage using vibration responses from a fleet of vehicles. In their studies, the features extracted by the autoencoders had a roughly linear relationship with the damage labels. Taking advantage of this, semi-supervised learning models were proposed to quantify the damage requiring only a few damage-labelled data; they greatly reduce the need for damage labels, increasing the method’s practicability. However, the performance of these methods relies on Machine Learning (ML) methods. Such methods usually lack a clear physical explanation, and they often demand the evaluation of dimensionality reduction/feature extraction methods (e.g., autoencoders) over raw dynamic measurements and sometimes strict parameter tuning. An important concern is that such approaches might bind the monitoring model to a particular structure or system, as features from ML techniques are often not applicable to different bridges [39]. Thus, this is also not conducive to the establishment of a comprehensive automatic monitoring system in general.

An ideal automated inspection can take vehicle responses as direct inputs (e.g., acceleration signals) to diagnose damage quickly and automatically with little or even no reliance on human guidance. There are some expectations for building a vehicle-based instant monitoring system. First, most existing research relies on the vehicle’s frequency-domain responses, and indirect SHM frameworks that use time-domain responses lack physical insights. Besides being inconvenient for automated inspection, another concern is that the transformation of signals from the time domain to the frequency domain can lead to information losses, which may be also related to the damage (especially for small or local damage) [40]. Hence, understanding the relationship between time-domain responses and bridge damage is pivotal. Second, the time-domain signals of vehicles can contain noise and data redundancy, etc. In order to ensure the efficiency and transferability of the SHM framework, the data processing methods should be efficient, universal, and less parameter-dependent. Third, since SHM is a highly responsible task and deficiencies from a drive-by measurement are inevitable, in addition to being automatic, the diagnostic model should be physics-guided, interpretable, and robust.

In this paper, a novel automatic physics-guided framework for indirect SHM that uses raw vehicle accelerations as inputs is proposed to diagnose possible damage in bridge structures. First, numerical studies are conducted to investigate the relationship between the time-domain response and bridge damage, based on which a new damage index is proposed for damage diagnosis. At the same time, it also explores the identification of damage locations and proposes a location index. Second, data processing methods to the raw vehicle acceleration data are presented, which include filtering and pooling procedures. Third, a novel physics-guided semi-supervised model is designed to automate the damage diagnosis process. Damage detection involves three aspects: (1) Damage indication, which aims to indicate the occurrence of damage; (2) Damage quantification, which seeks to estimate the damage severity; and (3) Damage localization, targeting the identification of the damage location. The proposed framework was validated using datasets acquired from laboratory experiments employing a scale vehicle model and a steel beam. Additionally, the superiority of the proposed damage index and the rationale for the proposed physics-guided approach were also demonstrated through comparisons with ML-based methods. The goal is to develop a physics-guided framework for indirect SHM that can use raw vehicle accelerations as direct inputs to achieve automated and accurate damage detection.

The originality of the work can be summarized as follows: Firstly, numerical studies are conducted to investigate the relationship between vehicle time-domain signals and bridge damage, based on which a new damage index is proposed. Secondly, it explores the identification of damage locations based on the proposed methodological framework, introducing a location index and a preliminary method for localizing damage. Thirdly, a physics-guided diagnosis framework for bridge health monitoring is designed. This framework incorporates a data processing algorithm to handle raw vehicle acceleration (e.g., data denoising) and an automatic damage detection model. Fourthly, the proposed damage index is compared with machine learning-extracted features, discussing the limitations of the latter and underscoring the rationale for the proposed physics-guided approach. Fifthly, through laboratory experiments, the feasibility of the proposed framework using raw vehicle accelerations in indicating damage occurrence, quantifying damage, and locating damage has been validated, a feat seldom achieved in previous studies.

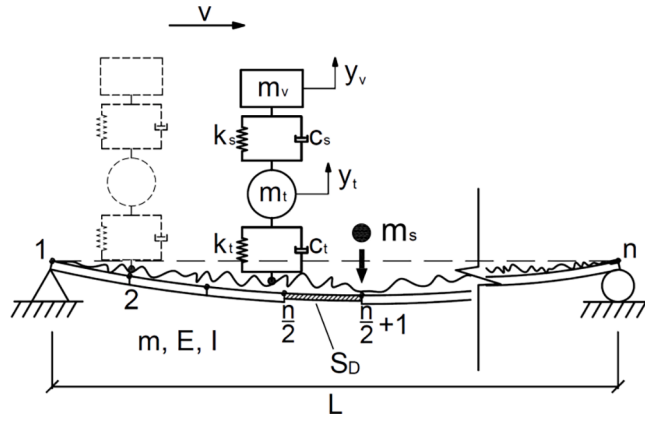


Fig. 1. VBI model.

2. Numerical study

2.1. VBI model

As mentioned in the introduction, numerical studies are conducted to provide a physical basis for the diagnosis framework. So far, several VBI models have been developed for numerical analysis. Some researchers have modelled vehicles as single vertical forces or a series of constant forces [41], while others have adopted a lumped sprung mass model [9,42]. More complex vehicle models include the 2-degree-of-freedom (DOF) quarter-car model, as well as 4-DOF models and so on [18,43,44]. In this study, the element-level coupling method is chosen using a 2-DOF vehicle model, in order to achieve a compromise between model complexity and computational efficiency, as shown in Fig. 1. The governing coupled equations for the VBI system are given by:

$$[M_v] \left\{ \ddot{u}_v \right\} + [C_v] \left\{ \dot{u}_v \right\} + [K_v] \{u_v\} = \{F_{cv}\} \tag{1}$$

$$[M_b] \left\{ \ddot{u}_b \right\} + [C_b] \left\{ \dot{u}_b \right\} + [K_b] \{u_b\} = \{F_{cb}\} \tag{2}$$

Equations (1) and (2) pertain to the motion equations for the vehicle and the bridge, respectively. The matrices $[M_v]$, $[C_v]$, and $[K_v]$ are related to the vehicle's mass, damping, and stiffness, while $[M_b]$, $[C_b]$, and $[K_b]$ signify the mass, damping, and stiffness matrices for the bridge model. Within the equations, $\{u_v\}$ denotes the displacement vector of the vehicle, while $\{u_b\}$ refers to the nodal displacement of the bridge system. Furthermore, $\{F_{cv}\}$ and $\{F_{cb}\}$ represent the time-dependent interaction forces on the vehicle and the bridge, respectively.

The vehicle model's matrices and response vectors can be presented as follows, where the body and axle masses are symbolized by m_v and m_t , the suspension and tire damping are represented by c_s and c_t , and the suspension and tire stiffnesses are denoted by k_s and k_t . The vertical displacements of the vehicle body and axle are portrayed by y_v and y_t , respectively.

$$[M_v] = \begin{bmatrix} m_v & \\ & m_t \end{bmatrix} \tag{3}$$

$$[C_v] = \begin{bmatrix} c_s & -c_s \\ -c_s & c_s + c_t \end{bmatrix} \tag{4}$$

$$[K_v] = \begin{bmatrix} k_s & -k_s \\ -k_s & k_s + k_t \end{bmatrix} \tag{5}$$

$$\{u_v\} = [y_v \quad y_t]^T \tag{6}$$

In the study, the road roughness is modelled in compliance with ISO 8608 [45], which can be represented using a power spectral density (PSD) function, as indicated in [46]:

$$G_d(n_s) = G_d(n_{s,0}) \left(\frac{n_s}{n_{s,0}} \right)^{-\alpha} \tag{7}$$

where n_s refers to the spatial frequency, and $n_{s,0}$ is the reference spatial frequency set at 0.1 m^{-1} . The constant α has a value of 2, and the roughness coefficient, $G_d(n_{s,0})$, is ascertained based on a variety of roughness classes. From Class A (best) to Class H (poorest), there

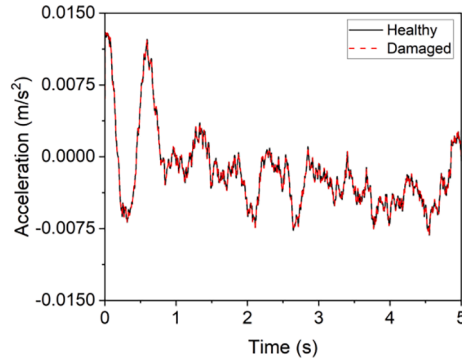


Fig. 2. Comparison of vehicle acceleration responses.

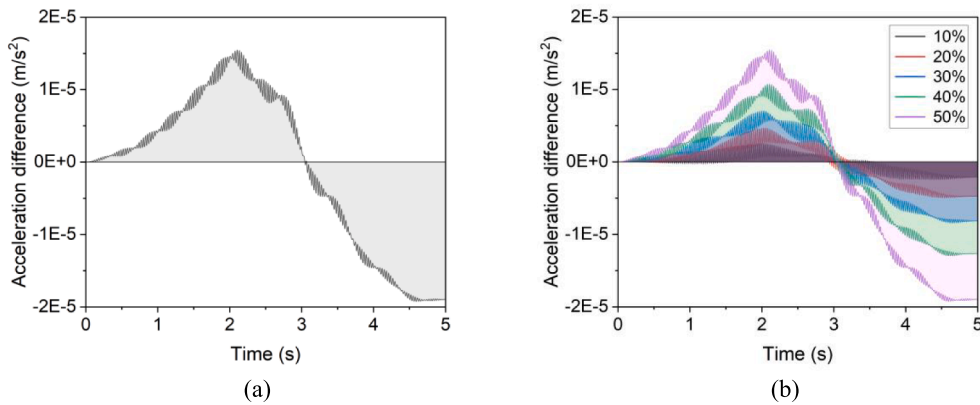


Fig. 3. Vehicle acceleration differences: (a) 50% damage severity, (b) 10% – 50% damage severity.

are eight classes associated with differing levels of road roughness [47]. For example, the geometric spatial means of Classes ‘A’, ‘B’ and ‘C’ profiles are $16 \times 10^{-6} \text{ m}^3$, $64 \times 10^{-6} \text{ m}^3$ and $256 \times 10^{-6} \text{ m}^3$, respectively.

A standard zero-mean real-valued stationary Gaussian process can then be used to simulate the surface roughness profile as follows:

$$r(x) = \sum_{i=0}^N \sqrt{2G_d(n_{s,i})} \Delta n_s \cos(2\pi n_{s,i}x + \theta_i) \tag{8}$$

In this equation, N represents the count of harmonic waves involved in constructing the roughness profile. $n_{s,i}$ indicates the i -th spatial frequency, while $\Delta n_s = 0.01 \text{ cycle/m}$ serves as the spatial frequency sampling interval. θ_i , the random phase angle for the i -th cosine function, is chosen uniformly at random from the range $[0, 2\pi]$.

The bridge is modelled as a simply supported Euler-Bernoulli beam, and each node of its FE model consists of 2 DOF (vertical translation and rotation). There are n elements, $n+1$ nodes and $2n$ DOF (excludes the constraints at both ends) in total. It has a length of L , a uniform flexural rigidity of EI , and a mass per unit length of m . The damping of the bridge is approximated by mass-stiffness proportional Rayleigh damping. Generally, bridge damage can be considered to be a loss of stiffness [48], which is given by:

$$S_D = S_H \times \varphi \tag{9}$$

where S_D is the damage severity (stiffness loss); S_H represents the intact stiffness and φ denotes the reduction of the stiffness of an element. This is often used to represent true bridge damage like cracks and delamination [49,50].

However, real damage should be avoided in experiments or field tests if possible, and the usual means is to add mass to the bridge to simulate the damage. The additional mass changes the mass of the bridge system and its dynamic characteristics [37], which can simulate changes in the physical properties of the bridge. Assuming that the bridge has an even number of elements, the mass matrix of the bridge model after placing the additional mass can be expressed as:

$$[M'_b] = [M_b] + \text{Diag}(0 \dots 0, m_s, 0 \dots 0) \tag{10}$$

where $\text{Diag}(\bullet)$ denotes the diagonal operator; the additional mass, m_s , is the n -th value (n -th DOF) in the diagonal operator and the rest

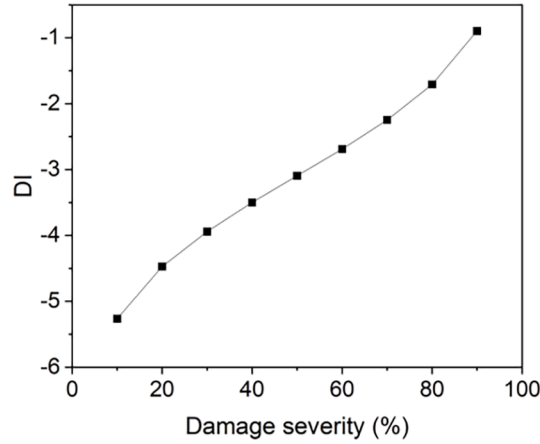


Fig. 4. Damage severity and its damage index, DI .

are zeros, which represents a concentrated mass added to the $(\frac{n}{2} + 1)$ -th node (midspan of the bridge) as the artificial damage.

The VBI process can be solved by employing the Newmark-Beta method to obtain the dynamic responses of vehicle. The parameters β and γ of the Newmark-Beta method are selected as 0.25 and 0.5, respectively, as suggested by many studies [13,46,51].

2.2. Numerical analysis of damage severity

The numerical analyses are performed based on a steel beam bridge, which can be regarded as a real-scale bridge of the laboratory beam model used in the study. The bridge parameters are: $m = 1250 \text{ kg/m}$, $EI = 2.6 \times 10^{12} \text{ N} \cdot \text{m}^2$, $L = 45 \text{ m}$ (the beam of length is divided into 10 elements, that is, $n = 10$), $f_{b,1} = 35.4 \text{ Hz}$ (the first modal frequency), and road profile class 'A'. It should be noted that the purpose of this section is only to verify the method but not to reproduce the actual behavior of the bridges. The initial vehicular parameters are adopted from McGetrick et al. [52] with some modifications, which can represent a truck or a bus, while the performance of the methodology will be demonstrated below to be less dependent on the car parameters. The initial vehicle parameters are: $m_v = 1.6 \times 10^4 \text{ kg}$, $m_t = 7 \times 10^3 \text{ kg}$, $c_s = 1.0 \times 10^4 \text{ N} \cdot \text{s/m}$, $c_t = 0$, $k_s = 4 \times 10^5 \text{ N/m}$, $k_t = 1 \times 10^4 \text{ N/m}$, and $v = 9 \text{ m/s}$. Since the goal of the diagnostic framework is to solve the real damage problem, the numerical studies will be mainly based on the stiffness loss as damage. As a simulated damage used in the laboratory, the use of mass increase will then be justified.

Fig. 2 presents the vehicle axle's acceleration responses, \ddot{y}_t , for the bridge in both healthy and damaged states (50 % stiffness loss); their time-domain responses have similar curve shapes. As shown in Fig. 3a, subtracting the accelerations of the damaged case from the healthy case yields a residual acceleration curve. As the damage becomes severer from 10 % to 50 %, the acceleration difference increases gradually (see Fig. 3b). The cumulative acceleration difference is calculated as (the area enclosed by the residual acceleration curve and the baseline):

$$\Delta A = \int_0^T \left(\left| \ddot{y}_H - \ddot{y}_D \right| \right) dt = \sum_{i=1}^N (|x_i^H - x_i^D|) \Delta t \quad (11)$$

where \ddot{y}_H and \ddot{y}_D are the vertical accelerations of the axle in healthy and damaged states, respectively; T denotes the total time for which the car is on the bridge. For discrete acceleration signals, x_i^D and x_i^H represent the i -th acceleration signal in the healthy and damaged states, respectively; and N stands for the total number of discrete accelerations contained in the passing time, T .

A new damage index can be defined as follows (symbols in the formula represent the same as above):

$$DI = \ln(\Delta A) = \ln \left[\sum_{i=1}^N (|x_i^H - x_i^D|) \Delta t \right] \quad (12)$$

Fig. 4 shows that there is an approximate linear relationship between DI and damage severity. Such an index considers the contributions of all acceleration amplitudes. It is a parameter-less index, which could be more sensitive to damage and more suitable for damage detection problems.

The above analytical findings are not limited to a particular vehicle configuration, and this is demonstrated using vehicle parameters chosen from a wide range, which can cover most commercial vehicle parameters. Fig. 5 shows that, despite changes in vehicle parameters, the connection between DI and damage severity is still approximately linear. Additionally, the adverse effects of road roughness are eliminated by the residual acceleration responses. It is also found that greater tire stiffness can be beneficial for damage detection since it provides higher DI values, which can reduce the requirement for the sensor's sensitivity, while other parameters have less effect on the DI value.

The above results show the relationship between DI and damage severity when stiffness loss is used as damage, which can represent

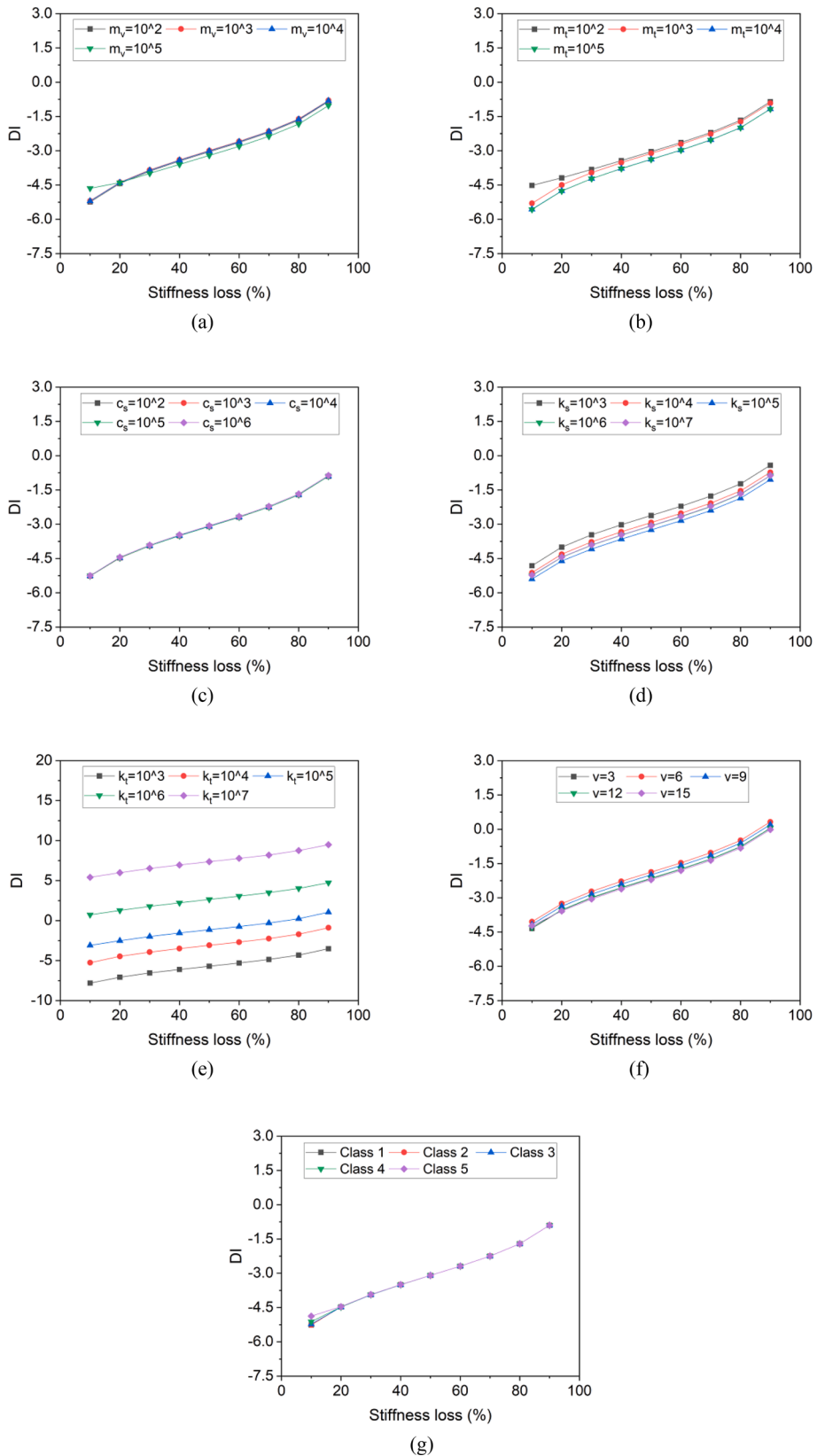


Fig. 5. Effects of vehicle parameters: (a) m_v , (b) m_t , (c) c_s , (d) k_s , (e) k_t , (f) v , (g) road roughness.

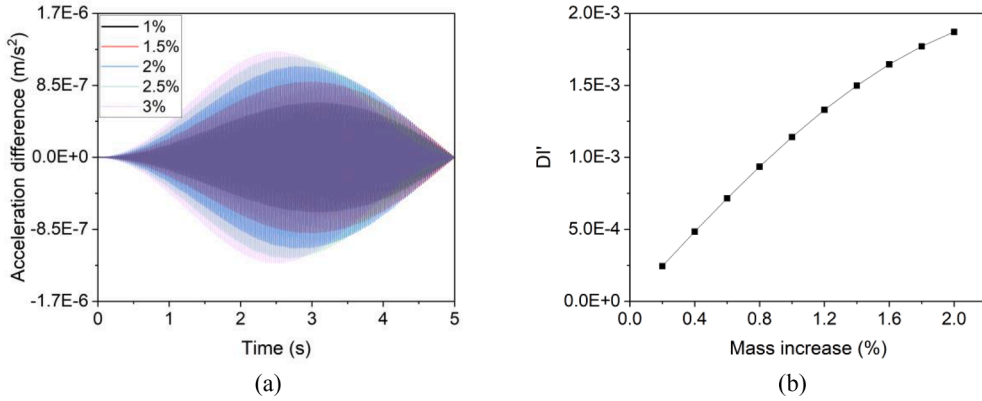


Fig. 6. Mass increase and its damage index: (a) residual acceleration, (b) DI' for mass increase.

the real damage [53]. To avoid permanent or irreversible destruction to the bridge, adding mass to it as artificial damage is a common practice in the laboratory [31,35,37]. Fig. 6a shows that the residual curve for mass increase is different to that of stiffness loss. However, it is noted that, when the mass increase is relatively small, its residual curve has a similar mode of change to that of stiffness loss (their areas grow in proportion). A damage index for mass increase can be defined by Eq. (13). When the mass increase is below 2 % of the bridge mass, the damage index, DI' , is roughly linear with the mass increase as the artificial damage (see Fig. 6b).

$$DI' = \Delta A = \sum_{i=1}^n (|x_i^H - x_i^D|) \Delta t \tag{13}$$

2.3. Investigation of damage location

Fig. 7a and Fig. 7b depict the residual acceleration curves for the 3rd and 7th beam elements from 10 % to 50 % damage, represented by 0.3L and 0.7L, respectively (the same below). It is evident that while their residual curves have a similar mode of change to those of the mid-span (the amplitudes grow proportionally), their “curve shapes” are different. Fig. 8 showcases the 50 % damage residual curves of all beam elements, from which the shape of the curve changes with the location of the damage. These indicate that the damage location correlates with the curve shape, while the damage severity is related with their amplitude.

A method to measure the similarity between two signals is the coherence, which can be mathematically given by Eq. (14) [54]. This measure serves to compare the relation between two signals. A coherence value of 1 indicates identical signals, whereas a value of 0 suggests complete dissimilarity. In this work, the average of the coherence values of the residual curves for two locations is used to represent their similarity (see Eq. (15), denoted as the location index (LI)).

$$C_{xy}(f) = \frac{|G_{xy}(f)|^2}{G_{xx}(f)G_{yy}(f)} \tag{14}$$

$$LI = E[C_{xy}(f)] \tag{15}$$

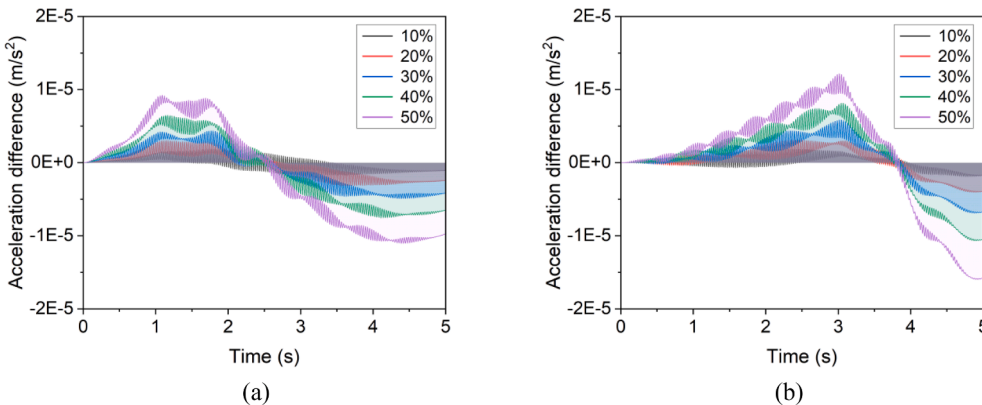


Fig. 7. Residual acceleration curves at different damage locations: (a) 0.3L, (b) 0.7L.

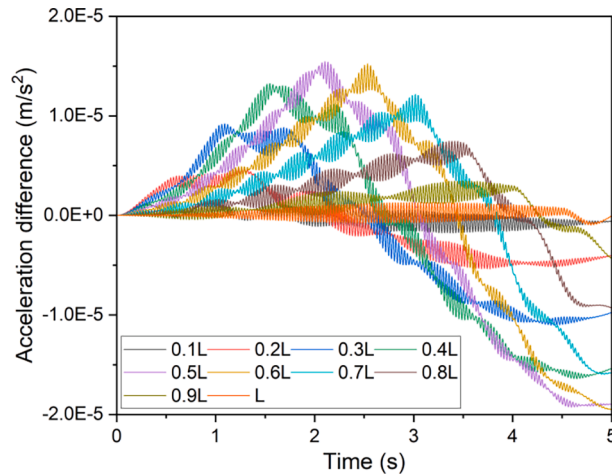


Fig. 8. Residual acceleration curves corresponding to the change of damage location.

where $G_{xy}(f)$ is the cross-spectral density of signals x and y , $G_{xx}(f)$ is the power spectral density of signal x , and $G_{yy}(f)$ is the power spectral density of signal y .

By calculating pairwise among different locations, a 10×10 matrix of the LI value can be obtained, as depicted in Fig. 9. It is evident that adjacent locations have higher LI values, with the LI value being 1 for identical locations. This index can serve to pinpoint the damage location. These are also applicable for cases where mass increase acts as artificial damage.

From the aforementioned analyses, the main insights are summarized as follows:

1. Damage on the bridge (e.g., stiffness loss) will change the amplitude of the vehicle’s acceleration response, affecting the entire time-domain response; the damage information is contained in every acceleration amplitude. A new damage index that considers the contributions of all acceleration amplitudes is proposed for evaluating damage levels.
2. Severer damage have a greater amplitude change in the vehicle’s acceleration responses, and there is a roughly linear relationship between the proposed damage index, DI , and the damage severity, which can be used to diagnose damage; the same applies to mass increase (less than 2 % in this study) as the artificial damage. These provide the basis for the algorithm below and justify the use of additional mass to simulate damage in the experiment.
3. The effects of vehicle parameters (e.g., mass and stiffness) and road roughness are eliminated by subtracting the acceleration responses over two runs (residual acceleration method) when computing the index, DI . So, this method does not require any specific vehicle configuration, but the same vehicle to travel on the same path at similar speeds throughout the tests.
4. The damage location correlates with the “shape” of residual acceleration curves, while the damage severity is related with their amplitude. By comparing the similarity in the shape of the residual curves, the damage can be located; they can be evaluated using the LI metric.

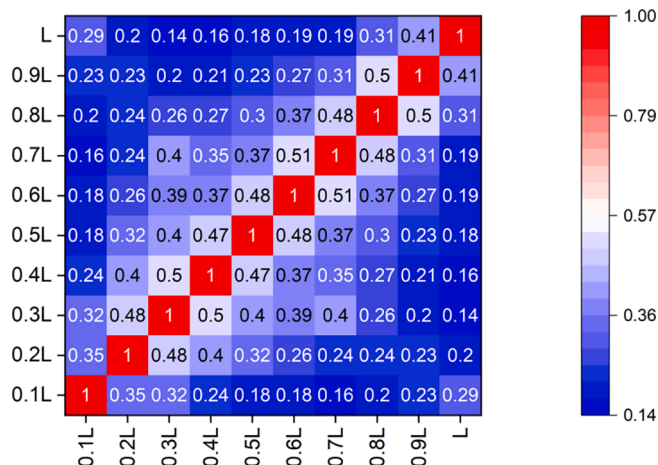


Fig. 9. LI matrix.

3. Damage diagnosis framework

The numerical study validates the feasibility of using the vehicle’s raw time-domain responses to diagnose damage and proposes a new damage index, DI for damage quantification. Additionally, it explores the issue of damage localization and proposes an LI metric for identifying the damage location. However, there are several challenges in applying this method in practice. For example, drive-by measurements inevitably contain noise/inaccuracies, ensuring a constant velocity is generally difficult, and the time-domain signals can be voluminous, demanding significant computational resources. To address these issues and to automate the SHM process, this section proposes a damage diagnosis framework. The designed framework consists of data processing methods and physics-guided semi-supervised models, aiming to apply the methodology proposed in the numerical study to practical engineering. The focus of the diagnostic model is on damage indication and quantification, while damage localization will be elaborated upon in the experimental analysis section. In the authors’ previous work, there were explorations on automated SHM models [55], but the model proposed in this study is more comprehensive. It has two stages: damage indication (stage I) and damage quantification (stage II). In stage I, only vehicle accelerations collected from a healthy bridge (health label) are required to train the model, while vehicle accelerations of a known damage severity (damage label) are also needed for model training in stage II. It can provide feedback to newly obtained raw vehicle acceleration data and automatically update the database, achieving automated damage detection of bridges.

It should be noted that this is an approach framework based on physical insights and statistical methods, in which typical ML operations are not performed; it is a physics-based diagnosis framework. Some terms of ML are used in the text to give readers a better understanding of the algorithmic processes only, such as clustering, semi-supervised models, pooling, and training.

3.1. Signal processing methods

A two-step data processing method for the raw vehicle acceleration data is proposed. It includes a filtering process and a pooling process, as presented in Fig. 10. The purpose of the filtering process is to denoise the raw data without altering its size. Utilizing the sliding window method, each signal in the input data is scanned with a template (or kernel, mask). The signal value is replaced based on a weighted average from its neighboring values, which is determined by a window function (see Eq. (16)). In the formula, i , denotes the i -th signal in the acceleration data, $S(i)$; w represents the length of the window function (or filter function), $W(n)$; the window function should be chosen based on the dominant noise. Given the predominance of white noise in the laboratory environment, a Gaussian function was chosen as the window function (see Eq. (17)). Its expected value, μ , is zero and the deviation, σ , is chosen to be 20 by trials. In fact, the function’s parameters do not significantly affect the results. It primarily removes the high-frequency noise in the signal, which is mainly related to the ambient noise [56]. The signal processing techniques investigated include Empirical Mode

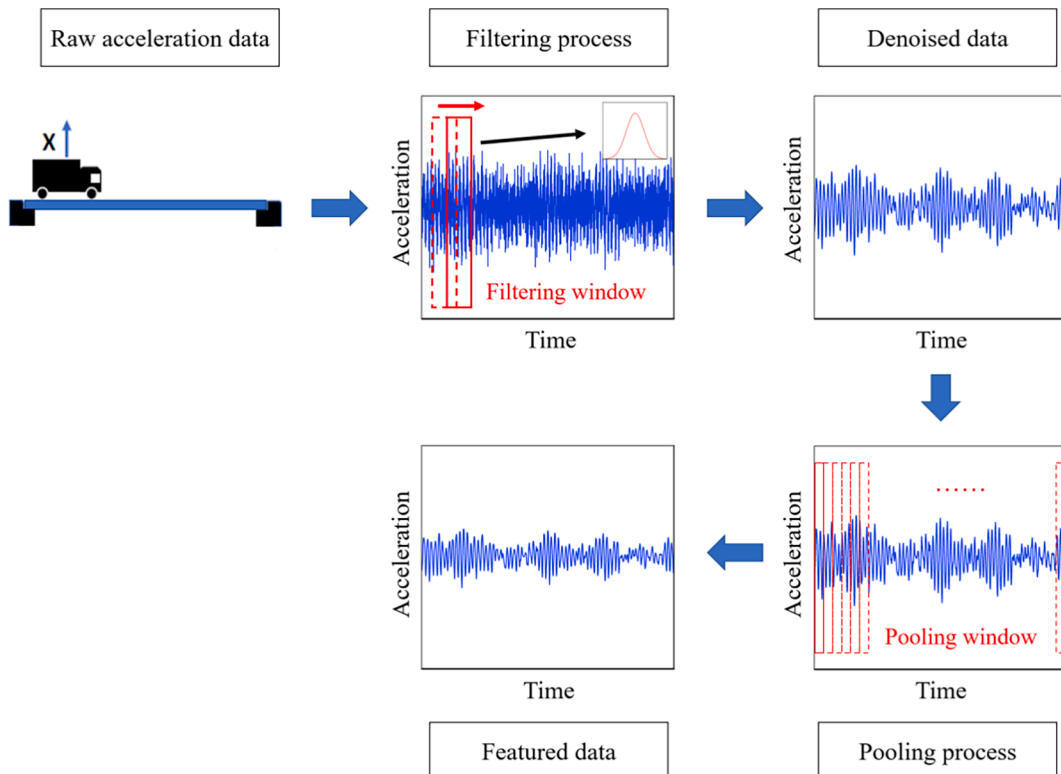


Fig. 10. Data processing methods.

Decomposition/ Ensemble Empirical Mode Decomposition (EMD/EEMD) and inverse Fourier transform (removing high-frequency data in the spectrum and then re-converting it to time-domain data), and the proposed method outperformed them.

$$f(i) = \sum_{n=1}^w S(i+n)W(n) \tag{16}$$

$$W(x) = \frac{1}{\sqrt{2\pi}\sigma} \exp\left(-\frac{(x-\mu)^2}{2\sigma^2}\right) \tag{17}$$

After filtering, the denoised data undergoes a pooling process, drawing inspiration from the pooling layer in neural networks [57]. This operation extracts the representative feature, such as the maximum or mean value, within a certain neighbourhood along the time-series direction. Even though pooling reduces data size, it mostly retains the data’s essential features [58], further reducing noise, normalizing data, and cutting computational expenses. As shown in Fig. 11, the two acceleration records (after the filtering process) are obtained by the same vehicle crossing the bridge repeatedly at speeds of v and $s \times v$, respectively. The passing time of the first run is T , sampled at frequency f , leading to a data size of $f \times T$. If the speed ratio for the other run compared to the first is s , then its data size becomes $(f \times T)/s$. This study employs max pooling to capture the peak value within a range, proving more insightful in real-world applications [59]. By adjusting the pooling window length, l , based on speed variations, the equal-sized data, $(f \times T)/l$, can be obtained. Although the pooling process can equalize the data size, the velocity difference should not be too large. A roughly 40 % speed variance is deemed tolerable based on prior findings [56,60]. Additionally, due to the reduced data redundancy, the diagnostic framework’s computational efficiency witnesses an improvement. The data size here is chosen to be 450, with each run automatically adjusting the window size (stride equals window length). Data that cannot be divided by 450 will have zeros appended to the end of it automatically. Simulation study indicates that the edge data scarcely affects the results. For a more detailed discussion on this data processing method, one can refer to the authors’ past work [61].

3.2. Physics-guided models for damage diagnosis

The diagnosis program has two stages: (1) damage indication; and (2) damage quantification. The first stage only requires vehicle accelerations recorded from healthy bridge as labelled data. After the collected accelerations are processed, they are fed into the clustering operation as inputs to find the cluster centre, O_H , which is considered as the representative of the health data (baseline). If there is a single cluster centre, it can be calculated using the formular:

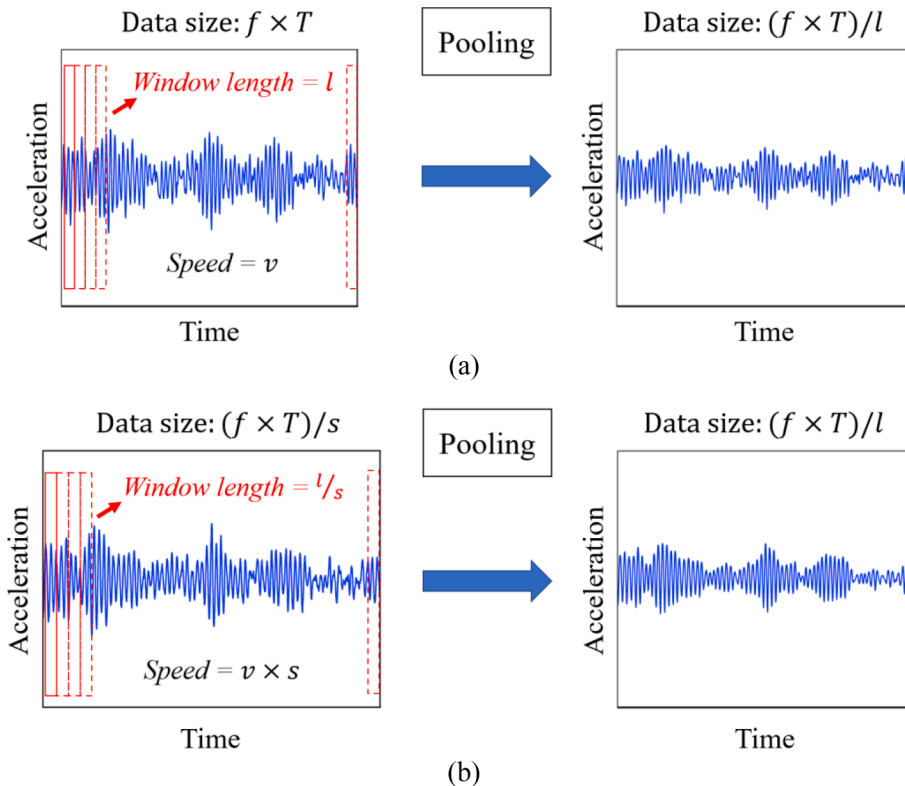


Fig. 11. Pooling process for vehicle acceleration records with different speeds: (a) v , (b) $s \times v$.

$$O_H = (1/|H|) \sum_{x^{(i)} \in H} x^{(i)}$$

where $|H|$ denotes the number of samples in the cluster H (healthy set); $x^{(i)}$ represents a labelled sample within the healthy set.

The analytical results in Section 2 suggest that the bridge health state can be diagnosed by the damage index, DI . Thus, the DI value for each sample in the healthy set is calculated using Eq. (13) and they are experimentally observed to be normally distributed. The threshold, DI_H , is defined as the DI value at the 95th percentile of the distribution (2σ), as shown in Fig. 12. In practice, some of the data that lies outside the 95 % interval may come from measurement errors. The above is referred to as the training phase, through which the baseline, O_H , and the threshold, DI_H , are acquired. In the detection phase, unlabelled data from the raw vehicle accelerations (after processing) are compared to the baseline, and if their DI values surpass the threshold, DI_H , an alarm will be triggered to inform a possible damage occurrence. Meanwhile, data that fall below the threshold will be labelled as healthy and used to update the health

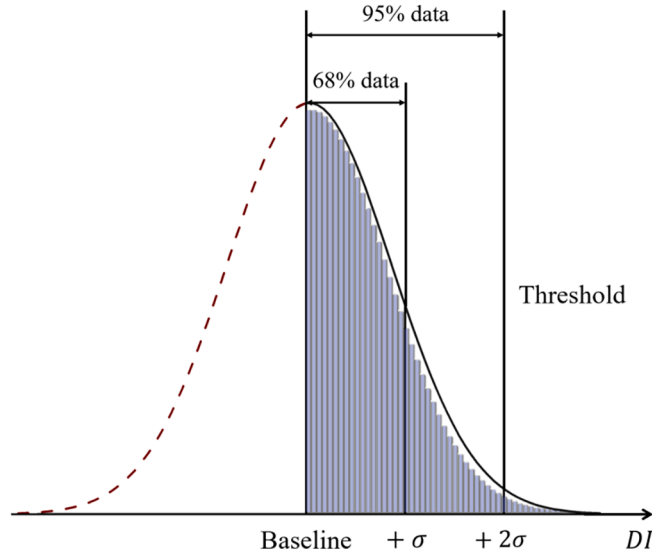


Fig. 12. The statistics distribution for DI .

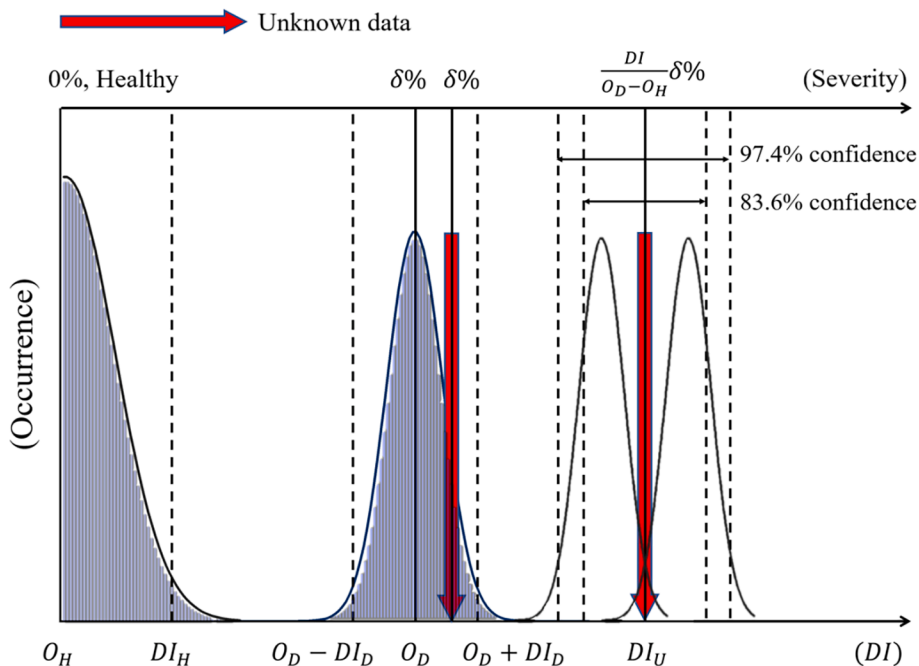


Fig. 13. Damage severity comparison.

dataset. Such a model can achieve instantaneous damage indication and automatic dataset updating when only health-labelled data are available. Health-labelled data are usually easier to access in engineering practice.

The second stage aims to quantify the damage severity. It requires labelled data of a known damage severity as input to train the clustering model, in addition to the health-labelled data. The training procedure is similar to that of the stage I, through which the damage point, O_D , and its ambit, DI_D , are obtained. The raw acceleration signals identified as damaged would be fed into the second diagnosis stage for severity estimation. As shown in Fig. 13, if a data falls within the ambits of the damage point, it will be recognized as that damage level ($\delta\%$) and then used to update the damage dataset and associated variables (e.g., the damage point and ambits); the input that does not fall into the known damage level will be sent into the damage severity comparison program.

As illustrated in Fig. 13, the DI value at the 95th percentile (2σ) is considered as the boundary of the damage distribution, and it is assumed that the unknown damage data have a similar distribution to the known damage. According to the results in Section 2, the damage severity is roughly proportional to the damage index, DI . Thus, a possible damage severity of the unknown data can be solved as:

$$S = \frac{DI_U}{O_D - O_H} \delta\% \tag{19}$$

where DI_U is the DI value of the unknown data; $\delta\%$ represents the known damage level (labelled data).

Considering that the input data may be located at the boundaries of two damage distributions at the same time, the possible severity range is determined by the two distributions, which is given by:

$$S_L^U = \frac{DI_U - 2DI_D}{O_D - O_H} \delta\% \tag{20}$$

$$S_R^U = \frac{DI_U + 2DI_D}{O_D - O_H} \delta\% \tag{21}$$

where S_L^U and S_R^U are the left and right boundaries of the severity range, respectively; O_D , DI_D , O_H , and $\delta\%$ represent the same as above, which are the damage point, its ambits (2σ boundary), the baseline, and the known damage level, respectively.

When the 2σ boundary is selected, the confidence is 97.4 % (there is a 97.4 % possibility that the damage event belongs to this severity range); the confidence is 83.6 % for the σ boundary ($DI_U \pm 1.5DI_D$). The processes described above can be encapsulated in an

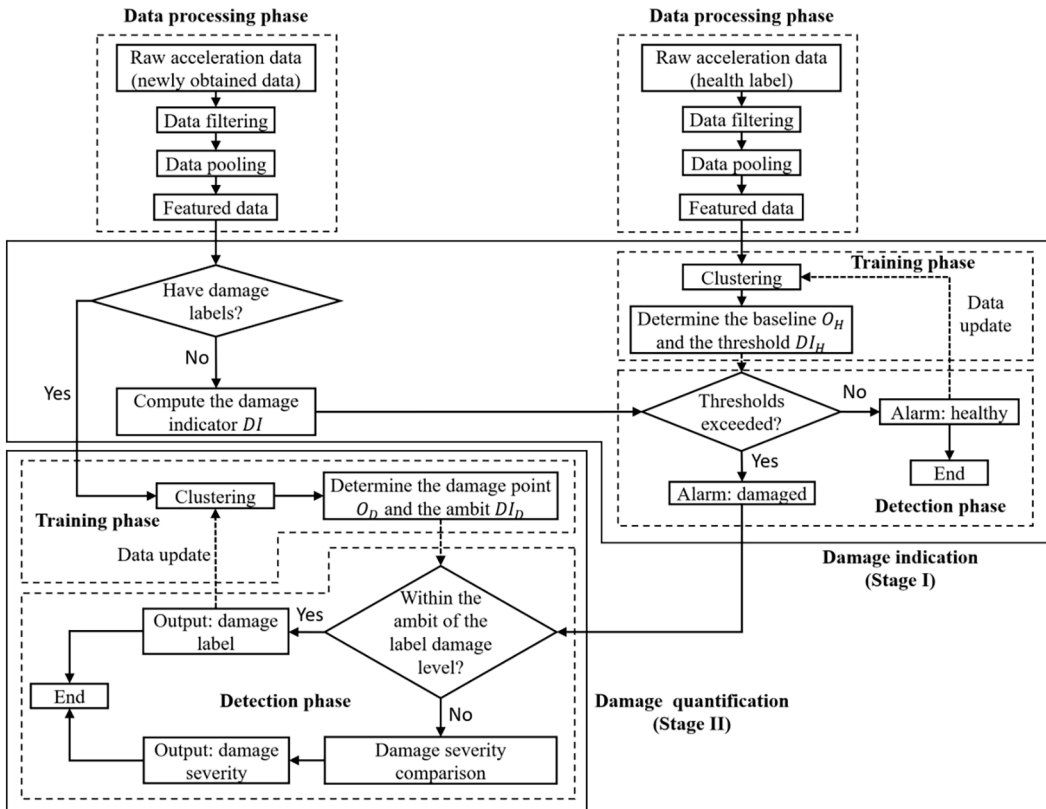


Fig. 14. Architecture of the damage diagnosis framework.

algorithmic framework, which is illustrated in Fig. 14.

It is worth mentioning that, obtaining data for a known damage level in real-world applications can be challenging. In response to this, the authors envision two possible solutions:

1. The occurrence of structural damage is usually a progressive process, and minor damage typically does not impose fatal harm to the structure. When minor damage appears in the structure, measurements can be taken to obtain the labelled data. This allows the current framework to be applied to diagnose subsequent damage and take preventive measures before severe damage emerges. In previous studies by the authors, the detection of minor damage was investigated, introducing methods such as the optimized AdaBoost-linear SVM [35] and the A2M-based approach [62]. These allow for the acquisition of minor damage information, subsequently providing labeled data for the methodology.
2. An alternative is leveraging Digital Twin technology to transfer damage sample data, simulated using finite element models, to measurements of experimentally tested structures and real bridge structures. However, it is crucial to ensure the fidelity of the data. Some efforts in this avenue include the works by Zhang et al. [63] and Teng et al [64].

4. Experimental study

4.1. Experimental program

Laboratory experiments were conducted to validate the present methodology, in which a steel beam and a scale truck model with an engine were employed. The acceleration data, collected from the vehicle sensor, were utilized to establish the dataset. As aforementioned, the damaged states were simulated by adding masses to the beam as “artificial damage”, thereby avoiding any permanent or irreversible destruction. The data acquisition system was managed via a PC and was connected to the sensors via wires, exhibiting a sampling rate of 2 kHz. Specifically, the sensors utilized in the experiments were made by Bruel & Kjaer (TYPE 4371) [65].

4.1.1. Bridge model

As shown in Fig. 15, the bridge model utilized in the experiment was a HEA400 simply supported steel beam. Physical properties of the steel beam are given as follows: elastic modulus $E = 199 \text{ GPa}$; density $\rho = 7.85 \times 10^3 \text{ kg/m}^3$; length $L = 4.4 \text{ m}$; section area $A =$

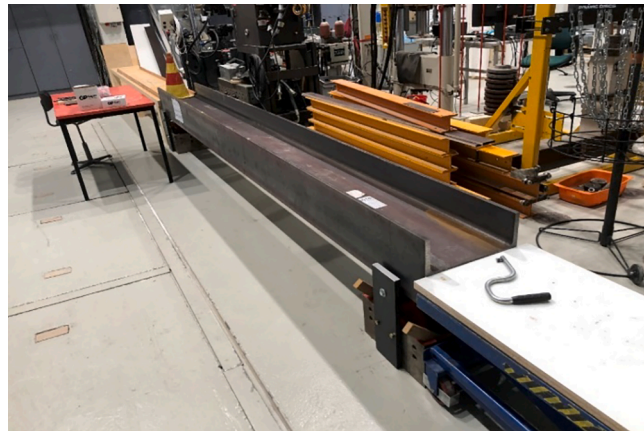


Fig. 15. Steel beam used as a bridge model.

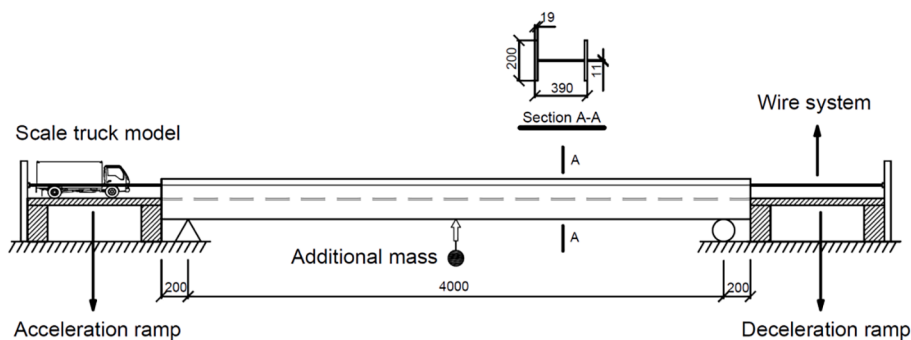


Fig. 16. Details of the bridge model (unit: mm).



Fig. 17. Setup for the lab test: (a) wire system, (b) added mass at the mid-span.

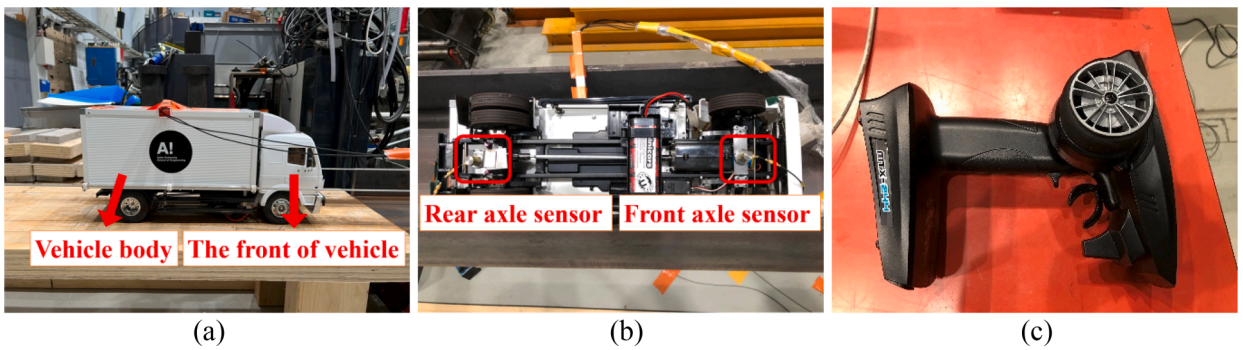


Fig. 18. Setup for the vehicle model: (a) scale vehicle model, (b) sensor installation on the vehicle, (c) electric controller.

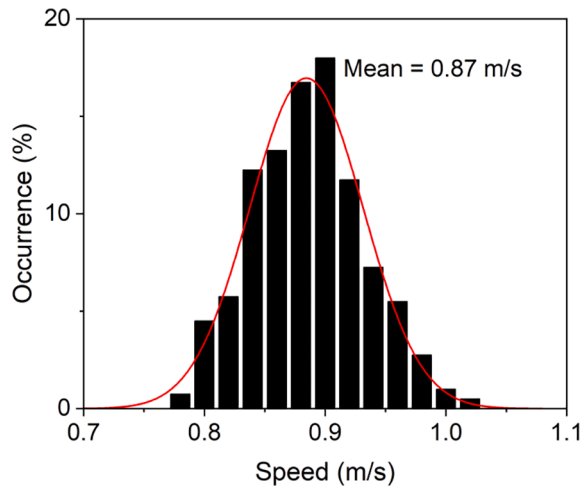


Fig. 19. Statistics distribution for speeds.

15898 mm² and moment of inertia $I = 8.564 \times 10^7 \text{ mm}^4$. The layout and sectional details of the beam model are shown in Fig. 16. The beam model has a first mode frequency of 35.4 Hz, which is measured by the direct method (placing sensors on the bridge). This beam model is approximately a lab-scale model for the bridge utilized in the numerical study. The experimental setup includes an acceleration ramp and a deceleration ramp, as well as a wire system that guides the vehicle to travel through the beam in a straight line and along the same path (see Fig. 17a). As shown in Fig. 17b, masses were added to the beam at the mid-span to generate damage cases, and a heavier mass indicates more severe damage. The details will be discussed later.

Table 1
Health state description.

Case No.	Weight	Runs	Type	Case No.	Weight	Runs	Type
0	0 (Healthy)	200	Label	3	6 kg (1.2 %)	50	Test
1	2 kg (0.4 %)	50	Test	4	10 kg (2 %)	50	Label
2	4 kg (0.8 %)	50	Test				

4.1.2. Vehicle model

As presented in Fig. 18a, the Tamiya Mercedes-Benz 1850L was used as the scale vehicle model in the study. This 1/14 scale model (568 mm × 202 mm) closely mirrors the design of a full-sized truck, with the exception of its weight. The vehicle's weight, determined experimentally, was 4.05 kg, accounting for 0.8 % of the bridge's total mass. Two accelerometers were strategically positioned on the front and rear axles, as illustrated in Fig. 18b. An added 5 kg weight was situated within the vehicle, bringing its total weight to 9.05 kg. Additionally, a 540-brushed type motor was utilized to drive the car model, operated by a remote controller, as shown in Fig. 18c. According to the numerical analysis, the method's sole requirement for the vehicle is that the dataset should be built by the same car, without needing any specific vehicle configuration. It is recommended that a similar or identical speed be maintained during different trials, and that an appropriate and relatively low speed be selected [18]. A too-low speed might not provide ample vehicle-induced excitation to provoke a strong enough VBI response. Conversely, exceedingly high speeds (akin to highway velocities) might result in a transient passage time, preventing the bridge from undergoing a full vibrational cycle [10,27]. An important concern is that too-different velocities could excite distinct modes of the bridge, thereby potentially influencing detection performance. Fig. 19 shows the velocity statistics from the experiment, approximately adhering to a normal distribution. Velocity varied between 0.78 m/s and 1.02 m/s, with a maximum to minimum speed ratio of 130.8 % - well within the generally accepted 40 % variance [56,60]. The mean speed is 0.87 m/s. It can replicate a speed of approximately 32.4 km/h (or 9 m/s) on a 45 m-span simply supported bridge with similar properties [31], aligning with the speed used in the numerical study.

4.1.3. Experimental dataset

In the proposed method, the vehicle was driven across the bridge repeatedly to acquire the dataset. Initially, a dataset pertaining to damage located at the mid-span was collected to validate the damage diagnosis framework. A more diverse set of validation scenarios will be presented in the subsequent sections to explore the identification of damage locations and to examine the robustness of the framework across various scenarios. For the diagnosis framework, the acceleration signals of the vehicle collected from the bridge in a healthy state are required to be used as the label data in stage I. In addition to the health-labelled data, stage II also requires damage-labelled data from a known damage severity. The test data obtained from other three damage states were utilized as unknown data to verify the performance of the proposed method. A description of these cases can be found in Table. 1. The healthy state contains 200 vehicle runs while the others have 50 runs each, which can correspond to the fewer and unbalanced damage samples in practice. For each run, the signal segment with the whole car on the beam is selected as the input acceleration. Thus, there are 200 (runs) × 1 (cases) × 2 (sensors) = 400 (signals) for the healthy state and 50 (runs) × 4 (cases) × 2 (sensors) = 400 (signals) for the damaged state; the experimental dataset has 800 signals in total.

4.2. Results and analysis

In this section, the experimental results are shown to validate the performance of the proposed framework. There are four subsections in total. The first subsection seeks to indicate the occurrence of damage (stage I). The second subsection aims to estimate the damage severity (stage II). The third subsection compares the features from dimensionality reduction/feature extraction methods like Principal Component Analysis (PCA) to demonstrate the superiority of the proposed damage index. The fourth subsection demonstrates how to pinpoint the damage location using the proposed methodology, and further validate the robustness of the diagnostic framework.

4.2.1. Damage indication

This subsection involves data from three different health states (cases 0, 1, and 2). Case 0 as the health-labelled data is used to train the model, while others are utilized as test data (unknown input) to show the performance of the proposed method. The results from the rear axle sensor are illustrated in the 1st and 2nd subsections, while results from the front axle sensor will be discussed in the 3rd subsection. Since our experimental dataset is based on the artificial damage of mass increase, DI' is taken as the damage index at this time ($DI = DI'$), and the same is applied below. In the training phase, the threshold of the healthy state, DI_H , can be computed as 1.75×10^{-2} (95 % confidence), and the baseline is the coordinate origin. Fig. 20a shows a comparison between the healthy state and the case 1 (0.4 % mass increases). They roughly follow the normal distribution, and the statistics distributions of their DI values are close; the accuracy rate of damage identification is only 68 % in this case. While the DI values in the case 0 (healthy state) and the case 2 (0.8 % mass increase) are visually different (see Fig. 20b), in which the accuracy rate rises sharply to 100 %. These show that the present method is sensitive to structural change that is greater than 0.8 %. The task of this stage is to indicate the occurrence of damage on the bridge, and the identified damage will be sent to the next stage for severity qualifying.

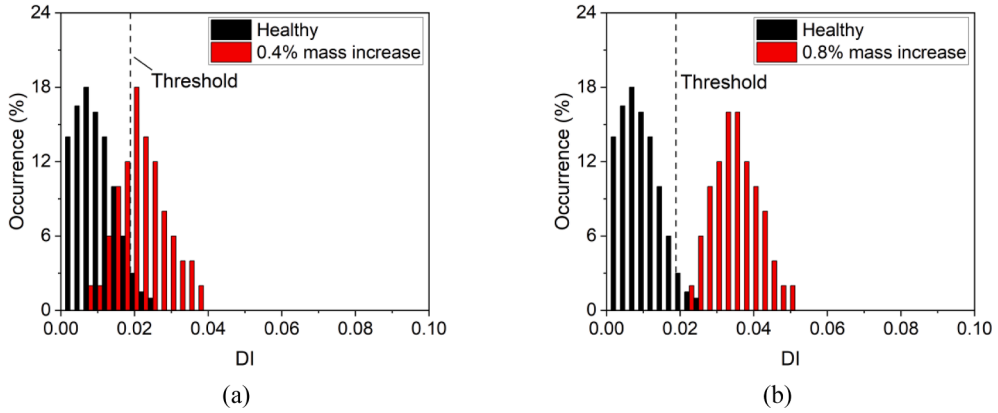


Fig. 20. Damage indication for different cases: (a) 0.4% mass increase, (b) 0.8% mass increase.

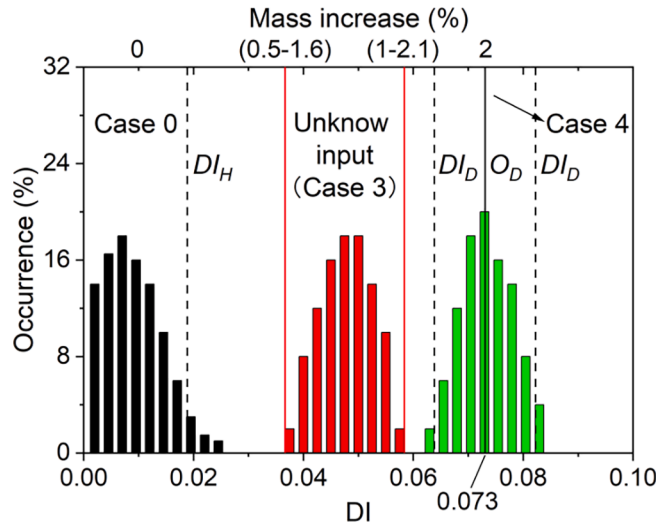


Fig. 21. Damage comparison.

4.2.2. Damage qualification

This stage focuses on the estimation of damage levels. Vehicle accelerations obtained from experiments with a 10 kg mass increase on the bridge are used as damage-labelled data (case 4) in addition to the health-labelled data (case 0). Cases 1, 2 and 3 are employed as testing data (unknown input) to illustrate the model’s performance on damage qualification. The damage point, O_D , and its ambit, DI_D , can be obtained as 7.3×10^{-2} and 9.9×10^{-3} (95 % confidence), respectively, through the training phase. When multiple data are available for the same damage severity, since they belong to the same distribution, the estimated damage severity should be an intersection. Given N pieces of data (vehicle passages), and each data corresponds to a severity range $R_i = [S_L^{U_i}, S_R^{U_i}]$, which can be computed using Eqs. (20) and (21). The intersection of these ranges, R^N , can be expressed by Eq. (22). This representation describes the intersection of the ranges from R_1 to R_N . In this study, N can be chosen from 1 to 50.

$$R^N = \bigcap_{i=1}^N R_i \tag{22}$$

In the detection phase, the damage levels (mass increases) for the left and right edge data of case 3 can be estimated as 0.5 %-1.6 % and 1 %-2.1 %, respectively (see Fig. 21). The damage level of case 3 should be $R^{50} = \bigcap_{i=1}^{50} R_i$, which is 1 % to 1.6 % (97.4 % confidence). When the confidence interval is reduced to 83.6 %, the severity range can be further estimated to be 1.15 %-1.45 %; the actual severity is 1.2 % (case 3), which lies within this range. For all test cases (e.g., cases 1, 2 and 3), their estimated severity range and actual severity are shown in the Fig. 22. The solid line in the figure is the actual severity, and the coloured area represents the estimated severity range. The results show that the present methodology can successfully estimate the severity for all cases, and there is a roughly linear relationship between the damage index, DI , and the actual severity, which verifies the findings from the numerical study. Furthermore, it can be found that increasing the number of measurements of the same state can improve the accuracy of damage estimation. In this study, for vehicle measurements ranging from 1 to 50, N of severity ranges are randomly select from R_1 to R_{50} to compute R^N . This

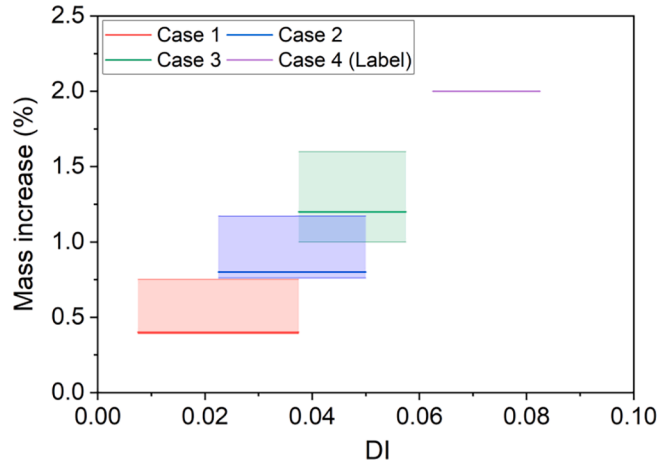


Fig. 22. Damage estimation for different cases.

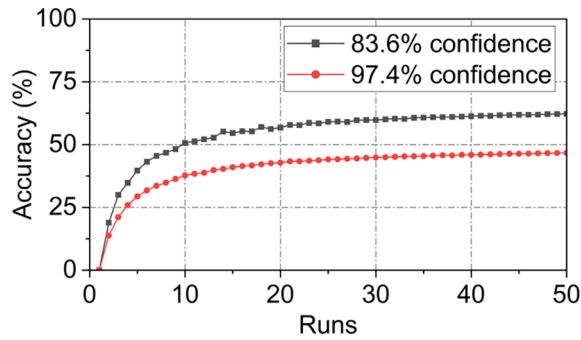


Fig. 23. Accuracy changes with vehicle passages.

process is repeated 2000 times. If $|R^{NM}|$ represents the length of the intersection obtained in the M -th iteration, then the average, $|\overline{R^N}|$, is given by Eq. (23). For example, with two vehicle measurements, R^{21} is the intersection of R_1 and R_2 , while R^{22} is the intersection of R_1 and R_3 , and so on. $|\overline{R^2}|$ represents the average range length of 2000 random combinations. Accuracy (or, its improvement) for the N passages in this study can be defined by Eq. (24). It refers to how close an estimated value/range is to the actual value.

$$|\overline{R^N}| = \frac{1}{2000} \sum_{M=1}^{2000} |R^{NM}| \tag{23}$$

$$Precision = \frac{|\overline{R^1}| - |\overline{R^N}|}{|\overline{R^1}|} \tag{24}$$

Fig. 23 illustrates that the accuracy in the case 3 generally increases with the number of vehicle measurements (similar results in other cases). Initially, the accuracy rises sharply with the increasing number of drives, but after 10 passages, the growth in accuracy starts to plateau. Nevertheless, multiple measurements are encouraged in engineering practice to enhance the accuracy of damage detection.

4.2.3. Comparison of feature extraction methods

To show the superior performance of the proposed damage index, it is compared with representative features extracted through different dimensionality reduction/feature extraction methods previously used in literature. These methods aim to find a low-dimensional representation of the correlation and distribution of acceleration signals collected from a passing vehicle [37,38,56]. In this study, PCA, Isomap, and Laplacian Eigenmaps (LE) are chosen as comparison methods. PCA is a linear dimensionality reduction technique that focuses on capturing the most variance in the data using eigenvectors of the dataset’s covariance matrix [66]. Isomap is a nonlinear dimensionality reduction method that seeks to maintain geodesic distances between data points, ideal for high-dimensional datasets with intricate relationships [67]. LE is a technique preserving the local structures by constructing a weighted graph from neighborhood data and utilizing its Laplacian matrix’s eigenvalues and eigenvectors for reduction [68].

To evaluate the clustering performance of different methods, the Root Mean Squared Errors (RMSE) of the representative features of acceleration signals are calculated as:

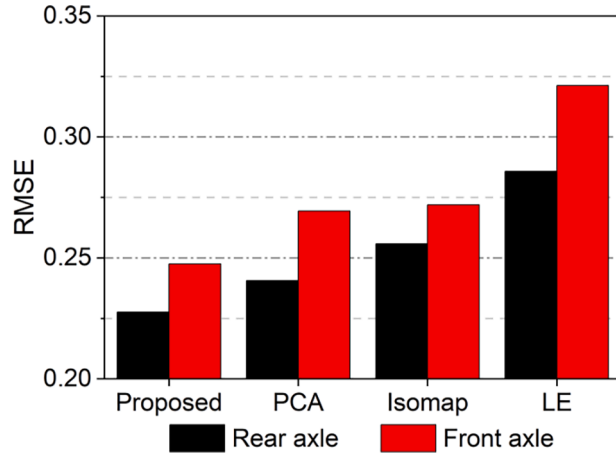


Fig. 24. RMSE results for different methods.

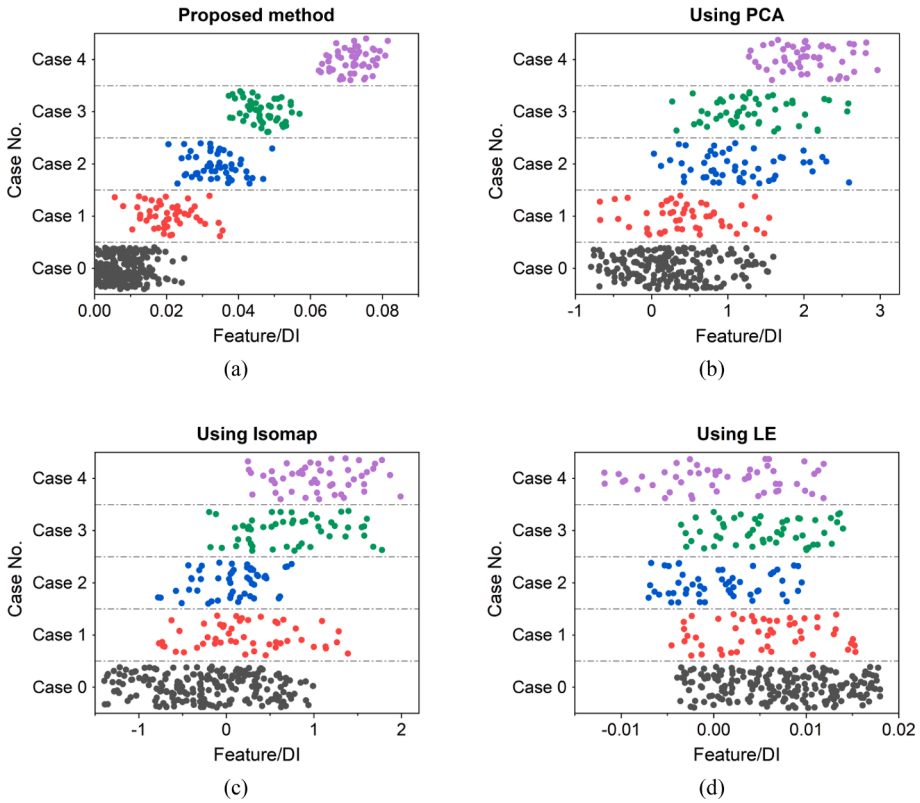


Fig. 25. Representative features obtained by different methods: (a) The proposed method, (b) PCA, (c) Isomap, (d) LE.

$$RMSE = \sqrt{(1/|C|) \left\{ \sum_{y^{(i)} \in C} \left[\frac{y^{(i)} - O_C}{y_{max} - y_{min}} \right]^2 \right\}}$$
25

where $|C|$ denotes the number of samples in the cluster C (test set); $y^{(i)}$ is the representative feature of the i -th sample learned by the dimensionality reduction method; O_C represents the cluster centre; y_{max} and y_{min} are the maximum and minimum values of y , respectively. The closer the RMSE value is to zero, the better the clustering of the data set, reflecting the “stability” of the feature.

In this subsection, the clustering performance of different methods is illustrated in cases 0–4. Fig. 24 presents the RMSE results for different methods on both the rear and front axles, which are the average values for all five cases. It can be observed that the proposed

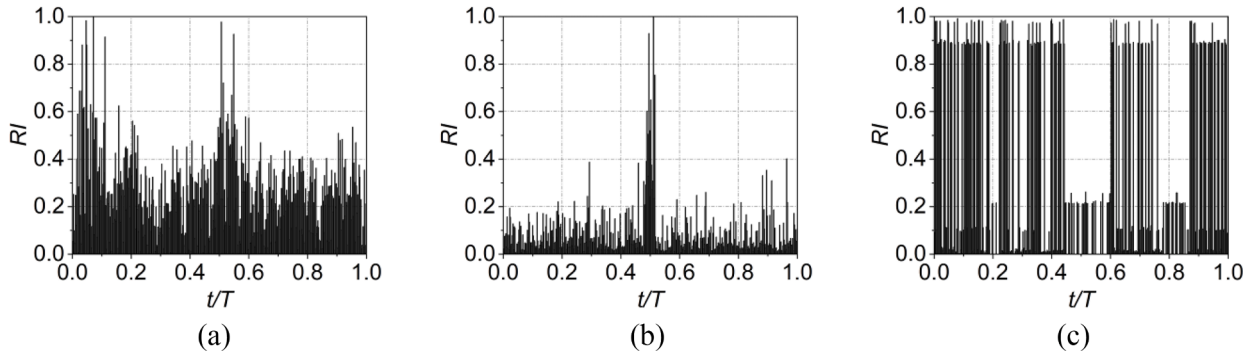


Fig. 26. RI for different ML techniques: (a) PCA, (b) Isomap, (c) LE.

method outperforms PCA, Isomap, and LE in terms of RMSE; the clustering performance of these methods is: Proposed method > PCA > Isomap > LE. Additionally, the results from the rear and front axle sensors are similar (or the rear axle results are slightly better than the front axle), indicating that the methodology's performance is not affected by the sensor position.

Fig. 25 illustrates the representative features learned by different methods from the time-domain signals of the rear axle sensor, and similar results can be seen in the front axle sensor. The result of the proposed method shows that the *DI*s of each case are concentrated in a cluster, making it possible to distinguish different health states. The results of PCA and Isomap show that they also tend to cluster, and the features shift with increasing masses to some extent. However, their performance is visually worse than that of the proposed method, where the health states cannot be clearly or easily distinguished. Among them, LE is deemed to perform the worst, and it is almost impossible to identify the health state from the extracted feature. In addition to the advantage of the proposed damage index, there are two reasons for these results. First, there are discontinuities between data samples in the experimental dataset, caused by experimental interruptions such as battery changes and setup adjustments (e.g., car track correction). Data discontinuities often occur in practice. The present dimensionality reduction methods are susceptible to discontinuities, with LE being the most vulnerable [37]. Second, the features extracted by the dimensionality reduction method can only represent a portion of the health state information and can be sensitive to outliers. The proposed damage index, *DI*, as a global feature, exhibits superior damage comparison results than the representative features learned by the other three methods on the experimental dataset.

Even though it is usually challenging to thoroughly interpret the features extracted using ML-based methods, a perturbation-based approach [69] can be employed to examine the 'contribution' of each acceleration data to these features, offering deeper insights into these ML methods.

In this approach, each acceleration data of the input is slightly perturbed. The difference (*Diff*) in the output between the perturbed and original input indicates the importance of that data point. Data points causing larger differences in the output are deemed more influential; this process is iteratively done for all acceleration data. In this study, the perturbation is set at 0.1 % of the maximum acceleration. For ease of comparison, their differences are displayed as Relative Importance (*RI*), which can be calculated using Eq. (26). In the equation, $Diff_{Min}$ and $Diff_{Max}$ represent the minimum and maximum *Diff* values in the output, respectively. They correspond to the acceleration at the normalized time, t/T , of the car traveling on the beam. When the vehicle is at the beginning and the end of the bridge, t/T equates to 0 and 1, respectively.

$$RI = \frac{Diff - Diff_{Min}}{Diff_{Max} - Diff_{Min}} \quad 26$$

Fig. 26 displays the *RI* in the representative features learned through different ML techniques, corresponding to the acceleration at the normalized time. In cases where the damage is represented by the mass at the midpoint (as seen in Fig. 6a), the central data points should contain more damage information ($t/T = 0.5$), while the data points at both ends should contain less ($t/T = 0, 1$). Fig. 26a reveals that, in the PCA method, the data points around $t/T = 0.5$ have a greater influence on the feature, which is reasonable. However, the points near $t/T = 0$ also demonstrate significant importance, indicating that a considerable portion of the feature information consists of noise rather than actual damage. Fig. 26b shows that Isomap seems to overly emphasize information at $t/T = 0.5$. However, damage information should be encompassed within the entire time domain signal. Overemphasis on localized data might not only overlook crucial damage information but also confront the peril of being tainted by local noise. As for the LE method, its focus, as shown in Fig. 26c, appears somewhat elusive, suggesting that this technique might not be well-suited for such problems; in fact, its performance was the worst. These indicate that features derived from ML techniques might not well represent or only capture a portion of the health status information. An inappropriate selection of ML methods could even lead to detection failures. Thus, the adoption of a physics-guided approach is rational.

Purity can be introduced as a metric to evaluate the clustering accuracy of the damage features [70]. It can be calculated using Eq. (27). The value of purity ranges between 0 and 1, with a higher value signifying greater accuracy in the clustering of the damage feature.

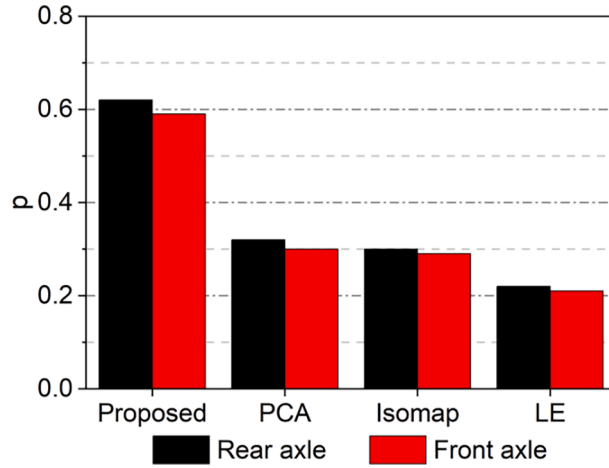


Fig. 27. Purity results for different methods.

Table 2
Validation cases.

	0.1L	0.3L	0.5L	0.7L	0.9L
0.0 %	Case 0 (Healthy)				
0.4 %	Case A1	Case B1	Case 1	Case C1	Case D1
0.8 %	Case A2	Case B2	Case 2	Case C2	Case D2
1.2 %	Case A3	Case B3	Case 3	Case C3	Case D3
2.0 %	Case A4	Case B4	Case 4	Case C4	Case D4

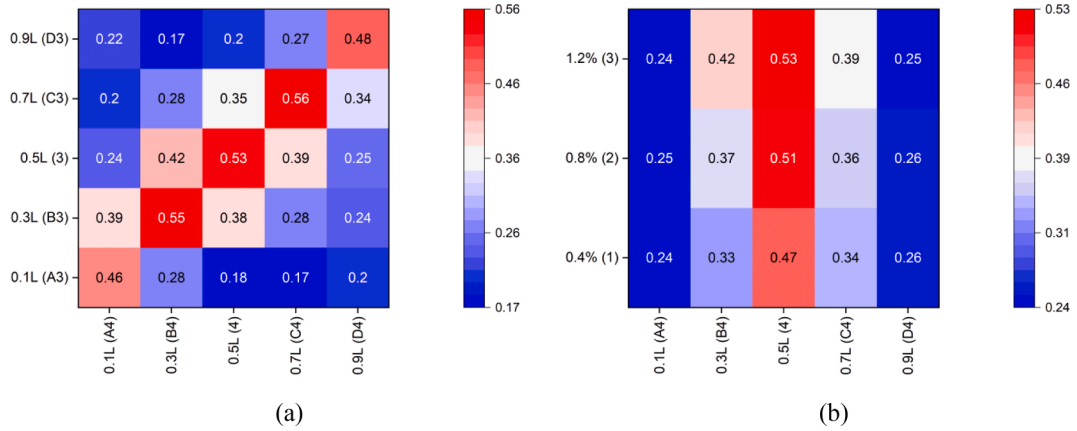


Fig. 28. LI matrix for validation cases: (a) diverse locations, (b) diverse severities.

$$p = \frac{1}{N_p} \sum_{i=1}^k \max_j |c_i \cap t_j|$$

27

where N_p denotes the total number of samples, k is the number of clusters, c_i is the i -th cluster, t_j represents the samples with the j -th true class label.

In Fig. 27, the purity results of different methods obtained from cases 0–4 are presented. Results from the rear and front axle sensors are similar. The proposed method outperforms PCA, Isomap, and LE, showing superior clustering accuracy. Their accuracies are: Proposed method > PCA > Isomap > LE.

4.2.4. Exploration of the damage location

The diagnostic framework has successfully indicated the occurrence of damage and quantified its severity. In this subsection, it aims to demonstrate how to pinpoint the damage location in the laboratory data set using the proposed methodology, and further

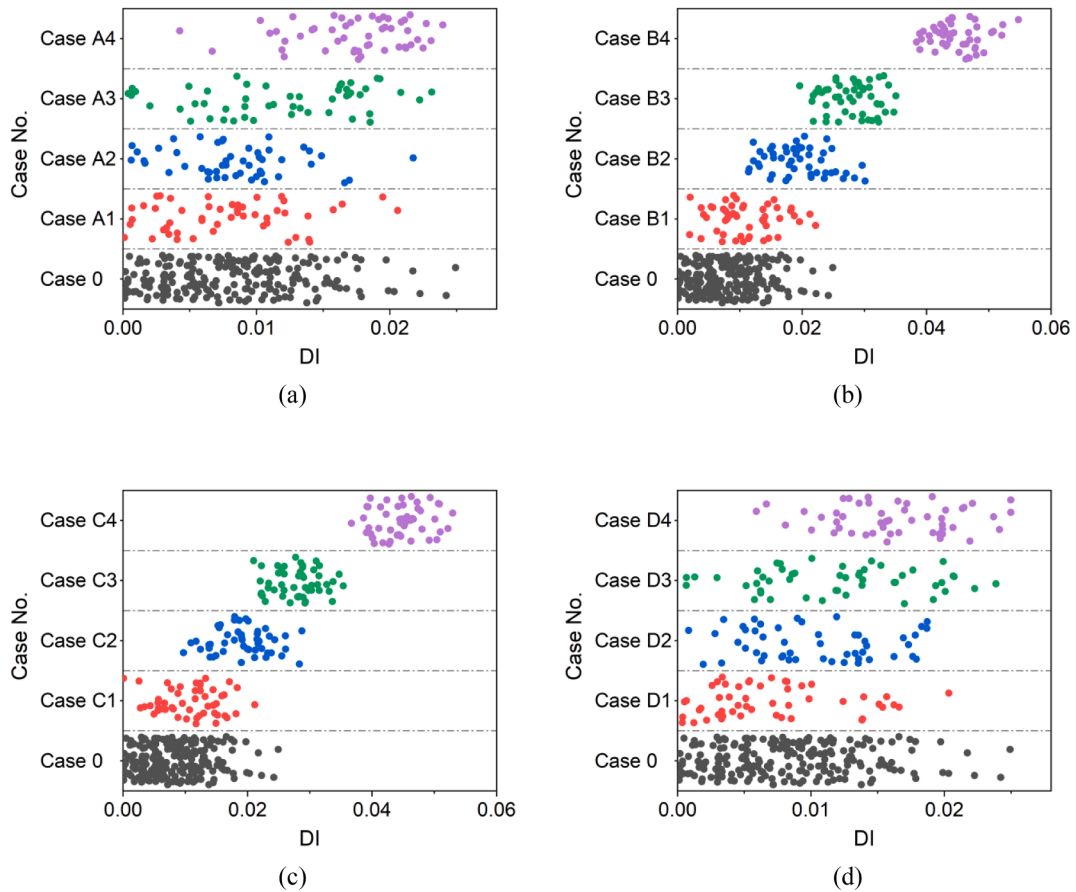


Fig. 29. Experimental results for different validation scenarios: (a) 0.1L, (b) 0.3L, (c) 0.7L, (d) 0.9L.

validate the robustness of the diagnostic framework across diverse scenarios. Here, in addition to the above cases 0, 1, 2, 3, and 4, new cases as detailed in Table 2 have been introduced. These represent the damage at 0.1L, 0.3L, 0.5L, 0.7L, and 0.9L of the beam, with severities of 0.4 %, 0.8 %, 1.2 %, and 2 % respectively. According to numerical investigation, close or identical damage locations should have similar residual curve shapes. This can be measured by *LI*, which is given by Eqs. (14) and (15). Fig. 28a delineates the *LI* matrix for various damage locations at a 1.2 % severity (cases A3, B3, 3, C3, and D3) in comparison with cases A4, B4, 4, C4, and D4 (2 % severity). Fig. 28b showcases the *LI* matrix for damage ranging from 0.4 % to 1.2 % at the midspan (cases 1 to 3) compared with cases A4, B4, 4, C4 and D4. They are all averages calculated from samples in these cases. It is evident that damage at the same location exhibit the highest *LI* values, followed by those at neighbour locations, which is true for different levels of damage. The location labels in cases A4, B4, 4, C4, and D4 are considered known in this study, then the damage locations in the remaining cases can be identified.

Fig. 29 displays the *DI* distributions across diverse scenarios obtained by varying the damage location. The positions 0.1L and 0.9L represent locations near the supports, while 0.3L and 0.7L signify regions closer to the mid-span. Evidently, the diagnostic approach exhibits superior performance for damage near the mid-span compared to those near the supports (their states are more easily discernible). At 0.3L and 0.7L, the damage of 0.8 % can be detected with accuracies of 72 % and 70 %, respectively, while at 0.1L and 0.9L, the damage of 2 % can only be detected with accuracies of 58 % and 46 %, respectively. This is predominantly because the damage near the supports induces particularly subtle changes, and typically, the drive-by method is insensitive to them. Overall, the performance of the framework is commendable, especially for damage near the midspan.

5. Concluding remarks

This paper proposes a physics-guided diagnosis framework for indirect SHM utilizing raw vehicle accelerations, which aims to achieve automated inspection of bridges. It consists of two parts. In the first part, a new damage index is obtained through numerical studies for bridge damage detection using vehicle time-domain signals. The index considers the contributions of all acceleration amplitudes and does not need any specific vehicle configuration. At the same time, it also explores the identification of damage locations and proposes a location index. To overcome deficiencies from a drive-by measurement and to automate the SHM process, a data processing method and a semi-supervised model are designed in the second part. Experiments were carried out to validate the proposed framework by utilizing a scale vehicle model and a steel beam. Based on the numerical and experimental results, the following

conclusions can be drawn:

- (1) There is a roughly linear relationship between the proposed damage index and the damage severity, which provides the potential to quantify the damage. The influences of vehicle parameters and road roughness can be eliminated when computing the damage index, thus they do not affect the detection results.
- (2) The damage location correlates with the “shape” of residual acceleration curves, while the damage severity is related with their amplitude. The proposed location index has been proven to successfully identify the location of the damage.
- (3) The proposed damage index and diagnostic framework are sensitive to damage. In the lab tests, the mid-span damage (structural change) to a degree of 0.8 % can be successfully detected; this is of great significance for the detection of minor damage.
- (4) In the diagnostic framework, the bridge damage can be quantified using raw vehicle accelerations. A large number of drive-by measurements can ensure more precise results in damage estimation, and this encourages multiple measurements to be performed in engineering practice.
- (5) The proposed damage index is shown to have better performance than the features from dimensionality reduction/feature extraction methods, such as PCA, Isomap, and Laplacian Eigenmaps. It demonstrates that features derived from ML techniques might not well represent or only capture a portion of the health status information.

This study validates the feasibility of automated inspection of bridges using only raw vehicle acceleration data. It provides the potential to achieve automatic, robust, and practical SHM systems toward a smart city/bridge. Future work will target the limitations of the proposed methodology. First, the present approach framework can accurately and automatically indicate the occurrence of damage and qualify its severity. It has also explored the identification of damage location. However, comprehensive and fully automated location identification still requires further development. Second, there is a need to verify the robustness of the diagnostic framework under more realistic and complex conditions, like a full-scale test in practice. A promising application would be on buses in daily operation, given their fixed routes and schedules, allowing for the collection of vast amounts of data on bridges within major urban areas.

Declaration of Competing Interest

The authors declare that they have no known competing financial interests or personal relationships that could have appeared to influence the work reported in this paper.

Data availability

Data will be made available on request.

Acknowledgments

This research is fully sponsored by the Jane and Aatos Erkkö Foundation in Finland (Grant No. 210018). The first author has also received financial support from the Chinese Scholarship Council (CSC) and the Finnish Foundation for Technology Promotion (TES).

References

- [1] O.A. Infrastructure, *A comprehensive assessment of America's infrastructure*, ASCE, 2021.
- [2] K. Gkoumas, F. Marques dos Santos, M. van Balen, A. Tsakalidis, A. Ortega, M. Grosso, A. Haq, F. Pekár, Research and innovation in bridge maintenance, inspection and monitoring A European perspective based on the Transport Research and Innovation Monitoring and Information System (TRIMIS), 2019. Doi: 10.2760/16174.
- [3] A.H. Alavi, M.Q. Feng, P. Jiao, Z. Sharif-Khodaei, Chapter 1 - Advanced sensing and monitoring systems for smart cities, in: A.H. Alavi, M.Q. Feng, P. Jiao, Z. Sharif-Khodaei (Eds.), *The Rise of Smart Cities*, Butterworth-Heinemann, 2022, pp. 1–26, <https://doi.org/10.1016/B978-0-12-817784-6.00012-6>.
- [4] Y. Gao, J. Meng, J. Shu, Y. Liu, BIM-based task and motion planning prototype for robotic assembly of COVID-19 hospitalisation light weight structures, *Automat. Construct.* 140 (2022), 104370, <https://doi.org/10.1016/j.autcon.2022.104370>.
- [5] S. Laflamme, F. Ubertini, A.D. Matteo, A. Pirrotta, M. Perry, Y. Fu, J. Li, H. Wang, T. Hoang, B. Glisic, L.J. Bond, M. Pereira, Y. Shu, K.J. Loh, Y. Wang, S. Ding, X. Wang, X. Yu, B. Han, Y. Goldfeld, D. Ryu, R. Napolitano, F. Moreu, G. Giardina, P. Milillo, Roadmap on measurement technologies for next generation structural health monitoring systems, *Meas. Sci. Technol.* 34 (2023), 093001, <https://doi.org/10.1088/1361-6501/acd135>.
- [6] C. Farrar, F. Hemez, D. Shunk, D. Stinematos, B. Nadler, A Review of Structural Health Monitoring Literature: 1996–2001, 2004.
- [7] M. Abdulkarem, K. Samsudin, F.Z. Rokhani, M.F.A. Rasid, Wireless sensor network for structural health monitoring: A contemporary review of technologies, challenges, and future direction, *Struct. Health Monit.* 19 (2020) 693–735, <https://doi.org/10.1177/1475921719854528>.
- [8] A. Malekjafarian, P.J. McGettrick, E.J. OBrien, A Review of Indirect Bridge Monitoring Using Passing Vehicles, *Shock Vib.* 2015 (2015), 286139, <https://doi.org/10.1155/2015/286139>.
- [9] Y.B. Yang, C.W. Lin, J.D. Yau, Extracting bridge frequencies from the dynamic response of a passing vehicle, *J. Sound Vib.* 272 (2004) 471–493, [https://doi.org/10.1016/S0022-460X\(03\)00378-X](https://doi.org/10.1016/S0022-460X(03)00378-X).
- [10] D. Hester, A. González, A discussion on the merits and limitations of using drive-by monitoring to detect localised damage in a bridge, *Mech. Syst. Sig. Process.* 90 (2017) 234–253, <https://doi.org/10.1016/j.ymssp.2016.12.012>.
- [11] A. Malekjafarian, E.J. OBrien, Identification of bridge mode shapes using Short Time Frequency Domain Decomposition of the responses measured in a passing vehicle, *Eng. Struct.* 81 (2014) 386–397, <https://doi.org/10.1016/j.engstruct.2014.10.007>.
- [12] E.J. OBrien, A. Malekjafarian, A mode shape-based damage detection approach using laser measurement from a vehicle crossing a simply supported bridge, *Struct. Control Health Monit.* 23 (2016) 1273–1286, <https://doi.org/10.1002/stc.1841>.
- [13] T. Nagayama, A.P. Reksowardojo, D. Su, T. Mizutani, Bridge natural frequency estimation by extracting the common vibration component from the responses of two vehicles, *Eng. Struct.* 150 (2017) 821–829, <https://doi.org/10.1016/j.engstruct.2017.07.040>.

- [14] D. Cantero, P. McGetrick, C.W. Kim, E. O'Brien, Experimental monitoring of bridge frequency evolution during the passage of vehicles with different suspension properties, *Eng. Struct.* 187 (2019) 209–219, <https://doi.org/10.1016/j.engstruct.2019.02.065>.
- [15] J. Li, X. Zhu, S. Law, B. Samali, Indirect bridge modal parameters identification with one stationary and one moving sensors and stochastic subspace identification, *J. Sound Vib.* 446 (2019) 1–21, <https://doi.org/10.1016/j.jsv.2019.01.024>.
- [16] Y.B. Yang, H. Xu, B. Zhang, F. Xiong, Z.L. Wang, Measuring bridge frequencies by a test vehicle in non-moving and moving states, *Eng. Struct.* 203 (2020), 109859, <https://doi.org/10.1016/j.engstruct.2019.109859>.
- [17] K. Feng, A. González, M. Casero, A kNN algorithm for locating and quantifying stiffness loss in a bridge from the forced vibration due to a truck crossing at low speed, *Mech. Syst. Sig. Process.* 154 (2021), 107599, <https://doi.org/10.1016/j.ymsp.2020.107599>.
- [18] M. Makki Alamdari, K.C. Chang, C.W. Kim, K. Kildashti, H. Kalhori, Transmissibility performance assessment for drive-by bridge inspection, *Eng. Struct.* 242 (2021), 112485, <https://doi.org/10.1016/j.engstruct.2021.112485>.
- [19] Y. Lan, W. Lin, Y. Zhang, Bridge Frequency Identification Using Multiple Sensor Responses of an Ordinary Vehicle, *Int. J. Struct. Stab. Dyn.* (2022) 2350056, <https://doi.org/10.1142/S0219455423500566>.
- [20] Y. Lan, W. Lin, Y. Zhang, Bridge frequency identification using vibration responses from sensors on a passing vehicle, in: *Bridge Safety, Maintenance, Management, Life-Cycle, Resilience and Sustainability*, CRC Press, 2022, <https://doi.org/10.1201/9781003322641-114>.
- [21] A. Di Matteo, D. Fiandaca, A. Pirrotta, Smartphone-based bridge monitoring through vehicle–bridge interaction: analysis and experimental assessment, *J Civil Struct Health Monit.* 12 (2022) 1329–1342, <https://doi.org/10.1007/s13349-022-00593-1>.
- [22] N. Shirzad-Ghaleroudkhani, M. Gül, Real-Life Investigations of Inverse Filtering for Frequency Identification of Bridges Using Smartphones in Passing Vehicles, in: *Lifelines 2022*, 2022: pp. 707–714.
- [23] J. Zhou, Z. Lu, Z. Zhou, C. Pan, S. Cao, J. Cheng, J. Zhang, Extraction of bridge mode shapes from the response of a two-axle passing vehicle using a two-peak spectrum idealized filter approach, *Mech. Syst. Sig. Process.* 190 (2023), 110122, <https://doi.org/10.1016/j.ymsp.2023.110122>.
- [24] Z. Li, Y. Lan, W. Lin, Indirect damage detection for bridges using sensing and temporarily parked vehicles, *Eng. Struct.* 291 (2023), 116459, <https://doi.org/10.1016/j.engstruct.2023.116459>.
- [25] Y. Lan, Z. Li, K. Koski, L. Fülöp, T. Tirkkonen, W. Lin, Bridge frequency identification in city bus monitoring: A coherence-PPI algorithm, *Eng. Struct.* 296 (2023), 116913, <https://doi.org/10.1016/j.engstruct.2023.116913>.
- [26] M. Bolognini, G. Izzo, D. Marchisotti, L. Fagiano, M.P. Limongelli, E. Zappa, Vision-based modal analysis of built environment structures with multiple drones, *Autom. Constr.* 143 (2022), 104550, <https://doi.org/10.1016/j.autcon.2022.104550>.
- [27] Y.B. Yang, J.P. Yang, State-of-the-Art Review on Modal Identification and Damage Detection of Bridges by Moving Test Vehicles, *Int. J. Struct. Stab. Dyn.* 18 (2018) 1850025, <https://doi.org/10.1142/S0219455418500256>.
- [28] Z.L. Wang, J.P. Yang, K. Shi, H. Xu, F.Q. Qiu, Y.B. Yang, Recent Advances in Researches on Vehicle Scanning Method for Bridges, *Int. J. Struct. Stab. Dyn.* (2022) 2230005, <https://doi.org/10.1142/S0219455422300051>.
- [29] A. Miyamoto, A. Yabe, Development of practical health monitoring system for short- and medium-span bridges based on vibration responses of city bus, *Journal of Civil, Struct. Health Monit.* 2 (2012) 47–63, <https://doi.org/10.1007/s13349-012-0017-0>.
- [30] E.J. O'Brien, P.J. McGetrick, A. González, A drive-by inspection system via vehicle moving force identification, *Smart Struct. Syst.* 13 (2014) 821–848, <https://doi.org/10.12989/sss.2014.13.5.821>.
- [31] C.W. Kim, R. Iseimoto, P.J. McGetrick, M. Kawatani, E.J. O'Brien, Drive-by bridge inspection from three different approaches, *Smart Struct. Syst.* 13 (2014) 775–796, <https://doi.org/10.12989/sss.2014.13.5.775>.
- [32] E.J. O'Brien, J. Keenahan, Drive-by damage detection in bridges using the apparent profile, *Struct. Control Health Monit.* 22 (2015) 813–825, <https://doi.org/10.1002/stc.1721>.
- [33] R. de Almeida Cardoso, A. Cury, F. Barbosa, Automated real-time damage detection strategy using raw dynamic measurements, *Eng. Struct.* 196 (2019), 109364, <https://doi.org/10.1016/j.engstruct.2019.109364>.
- [34] Q. Mei, M. Gül, N. Shirzad-Ghaleroudkhani, Towards smart cities: crowdsensing-based monitoring of transportation infrastructure using in-traffic vehicles, *J. Civil Struct. Health Monit.* 10 (2020) 653–665, <https://doi.org/10.1007/s13349-020-00411-6>.
- [35] Y. Lan, Y. Zhang, W. Lin, Diagnosis algorithms for indirect bridge health monitoring via an optimized AdaBoost-linear SVM, *Eng. Struct.* 275 (2023), 115239, <https://doi.org/10.1016/j.engstruct.2022.115239>.
- [36] A. Malekjafarian, F. Golpayegani, C. Moloney, S. Clarke, A Machine Learning Approach to Bridge-Damage Detection Using Responses Measured on a Passing Vehicle, *Sensors* 19 (2019) 4035, <https://doi.org/10.3390/s19184035>.
- [37] J. Liu, S. Chen, M. Bergés, J. Bielak, J.H. Garrett, J. Kovačević, H.Y. Noh, Diagnosis algorithms for indirect structural health monitoring of a bridge model via dimensionality reduction, *Mech. Syst. Sig. Process.* 136 (2020), 106454, <https://doi.org/10.1016/j.ymsp.2019.106454>.
- [38] M.Z. Sarwar, D. Cantero, Deep autoencoder architecture for bridge damage assessment using responses from several vehicles, *Eng. Struct.* 246 (2021), 113064, <https://doi.org/10.1016/j.engstruct.2021.113064>.
- [39] J. Liu, B. Chen, S. Chen, M. Bergés, J. Bielak, H.Y. Noh, Damage-Sensitive and Domain-Invariant Feature Extraction for Vehicle-Vibration-Based Bridge Health Monitoring, in: *ICASSP 2020 - 2020 IEEE International Conference on Acoustics, Speech and Signal Processing (ICASSP)*, 2020: pp. 3007–3011. Doi: 10.1109/ICASSP40776.2020.9053450.
- [40] D. Baglee, E. Jantunen, I. El-Thalji, T. Lagö, Problems with using Fast Fourier Transform for rotating equipment: Is it time for an update?, 2014. Doi: 10.13140/2.1.2679.1363.
- [41] S.P. Brady, E.J. O'Brien, A. Žnidarič, Effect of Vehicle Velocity on the Dynamic Amplification of a Vehicle Crossing a Simply Supported Bridge, *J. Bridge Eng.* 11 (2006) 241–249. Doi: 10.1061/(ASCE)1084-0702(2006)11:2(241).
- [42] Y.B. Yang, C.W. Lin, Vehicle–bridge interaction dynamics and potential applications, *J. Sound Vib.* 284 (2005) 205–226, <https://doi.org/10.1016/j.jsv.2004.06.032>.
- [43] P. Seetapan, S. Chucheeprakul, Dynamic responses of a two-span beam subjected to high speed 2DOF sprung vehicles, *Int. J. Struct. Stab. Dyn.* 6 (2006) 413–430, <https://doi.org/10.1142/S0219455406002015>.
- [44] J. Keenahan, E.J. O'Brien, P.J. McGetrick, A. González, The use of a dynamic truck–trailer drive-by system to monitor bridge damping, *Struct. Health Monit.* 13 (2014) 143–157, <https://doi.org/10.1177/1475921713513974>.
- [45] P. Múčka, Simulated Road Profiles According to ISO 8608 in Vibration Analysis, *J. Test. Eval.* 46 (2018) 20160265, <https://doi.org/10.1520/JTE20160265>.
- [46] H. Xu, Y.H. Liu, Z.L. Wang, K. Shi, B. Zhang, Y.B. Yang, General contact response of single-axle two-mass test vehicles for scanning bridge frequencies considering suspension effect, *Eng. Struct.* 270 (2022), 114880, <https://doi.org/10.1016/j.engstruct.2022.114880>.
- [47] Y.B. Yang, Y.C. Lee, K.C. Chang, Effect of Road Surface Roughness on Extraction of Bridge Frequencies by Moving Vehicle, in: A.K. Belyaev, H. Irschik, M. Krommer (Eds.), *Mechanics and Model-Based Control of Advanced Engineering Systems*, Springer, Vienna, 2014, pp. 295–305, https://doi.org/10.1007/978-3-7091-1571-8_32.
- [48] J.K. Sinha, M.I. Friswell, S. Edwards, SIMPLIFIED MODELS FOR THE LOCATION OF CRACKS IN BEAM STRUCTURES USING MEASURED VIBRATION DATA, *J. Sound Vib.* 251 (2002) 13–38, <https://doi.org/10.1006/jsvi.2001.3978>.
- [49] W.M. Ostachowicz, M. Krawczuk, On Modelling of Structural Stiffness Loss Due to Damage, *Key Eng. Mater.* 204–205 (2001) 185–200, <https://doi.org/10.4028/www.scientific.net/KEM.204-205.185>.
- [50] P. Shyamala, S. Mondal, S. Chakraborty, Numerical and experimental investigation for damage detection in FRP composite plates using support vector machine algorithm, *Structural Monitoring and Maintenance.* 5 (2018) 243–260, <https://doi.org/10.12989/smm.2018.5.2.243>.
- [51] C.W. Lin, Y.B. Yang, Use of a passing vehicle to scan the fundamental bridge frequencies: An experimental verification, *Eng. Struct.* 27 (2005) 1865–1878, <https://doi.org/10.1016/j.engstruct.2005.06.016>.
- [52] P.J. McGetrick, A. González, E.J. O'Brien, Theoretical investigation of the use of a moving vehicle to identify bridge dynamic parameters, *Insight - Non-Destructive Testing and Condition Monitoring.* 51 (2009) 433–438. <https://doi.org/10.1784/insi.2009.51.8.433>.

- [53] A. Malekjafarian, R. Corbally, W. Gong, A review of mobile sensing of bridges using moving vehicles: Progress to date, challenges and future trends, *Structures*. 44 (2022) 1466–1489, <https://doi.org/10.1016/j.istruc.2022.08.075>.
- [54] J.S. Bendat, A.G. Piersol, *Random data: analysis and measurement procedures*, John Wiley & Sons, 2011.
- [55] Y. Lan, Z. Li, W. Lin, Automatic Drive-By Bridge Damage Detection via a Clustering Algorithm, in: *Experimental Vibration Analysis for Civil Engineering Structures*, Springer Nature, Switzerland, Cham, 2023, pp. 144–154, https://doi.org/10.1007/978-3-031-39117-0_15.
- [56] Q. Mei, M. Gül, M. Boay, Indirect health monitoring of bridges using Mel-frequency cepstral coefficients and principal component analysis, *Mech. Syst. Sig. Process.* 119 (2019) 523–546, <https://doi.org/10.1016/j.ymsp.2018.10.006>.
- [57] D. Yu, H. Wang, P. Chen, Z. Wei, Mixed Pooling for Convolutional Neural Networks, in: D. Miao, W. Pedrycz, D. Ślęzak, G. Peters, Q. Hu, R. Wang (Eds.), *Rough Sets and Knowledge Technology*, Springer International Publishing, Cham, 2014: pp. 364–375. https://doi.org/10.1007/978-3-319-11740-9_34.
- [58] I. Goodfellow, Y. Bengio, A. Courville, *Deep Learning*, MIT Press, 2016.
- [59] N. Ketkar, *Deep Learning with Python*, Apress, Berkeley, CA, 2017. 10.1007/978-1-4842-2766-4.
- [60] A. Thorsen, G. Lederman, Y. Oshima, J. Bielak, H.Y. Noh, Mitigating the effects of variable speed on drive-by infrastructure monitoring, in: *Sensors and Smart Structures Technologies for Civil, Mechanical, and Aerospace Systems 2015*, SPIE, 2015: pp. 75–83. <https://doi.org/10.1117/12.2084435>.
- [61] Y. Lan, Z. Li, W. Lin, A Time-Domain Signal Processing Algorithm for Data-Driven Drive-by Inspection Methods: An Experimental Study, *Materials*. 16 (2023) 2624, <https://doi.org/10.3390/ma16072624>.
- [62] Z. Li, Y. Lan, W. Lin, Investigation of Frequency-Domain Dimension Reduction for A2M-Based Bridge Damage Detection Using Accelerations of Moving Vehicles, *Materials*. 16 (2023) 1872, <https://doi.org/10.3390/ma16051872>.
- [63] Y. Zhang, Z. Li, R. Hao, W. Lin, L. Li, D. Su, High-fidelity time-series data synthesis based on finite element simulation and data space mapping, *Mech. Syst. Sig. Process.* 200 (2023), 110630, <https://doi.org/10.1016/j.ymsp.2023.110630>.
- [64] S. Teng, X. Chen, G. Chen, L. Cheng, Structural damage detection based on transfer learning strategy using digital twins of bridges, *Mech. Syst. Sig. Process.* 191 (2023), 110160, <https://doi.org/10.1016/j.ymsp.2023.110160>.
- [65] Type 4371 Piezoelectric Charge Accelerometer | Brüel & Kjær, (n.d.). <https://www.bksv.com/en/transducers/vibration/accelerometers/charge/4371> (accessed October 2, 2022).
- [66] T. Hastie, R. Tibshirani, J.H. Friedman, *The elements of statistical learning: data mining, inference, and prediction*, 2nd ed, Springer, New York, 2009.
- [67] J.B. Tenenbaum, V. de Silva, J.C. Langford, A Global Geometric Framework for Nonlinear Dimensionality Reduction, *Science* 290 (2000) 2319–2323, <https://doi.org/10.1126/science.290.5500.2319>.
- [68] M. Belkin, P. Niyogi, Laplacian Eigenmaps for Dimensionality Reduction and Data Representation, *Neural Comput.* 15 (2003) 1373–1396, <https://doi.org/10.1162/089976603321780317>.
- [69] M. Ivanovs, R. Kadikis, K. Ozols, Perturbation-based methods for explaining deep neural networks: A survey, *Pattern Recogn. Lett.* 150 (2021) 228–234, <https://doi.org/10.1016/j.patrec.2021.06.030>.
- [70] A.K. Jain, M.N. Murty, P.J. Flynn, Data clustering: a review, *ACM Comput. Surv.* 31 (1999) 264–323, <https://doi.org/10.1145/331499.331504>.